Available online at www.sciencedirect.com
ScienceDirect
Vaccine 25 (2007) 630–637
Vaccine
www.elsevier.com/locate/vaccine

SARS-CoV spike protein-expressing recombinant vaccinia virus efficiently induces neutralizing antibodies in rabbits pre-immunized with vaccinia virus

Masahiro Kitabatake [a,b], Shingo Inoue [c], Fumihiko Yasui [a], Shoji Yokochi [a,d], Masaaki Arai [a,e], Kouichi Morita [c], Hisatoshi Shida [f], Minoru Kidokoro [g], Fukashi Murai [d], Mai Quynh Le [h], Kyosuke Mizuno [i], Kouji Matsushima [b], Michinori Kohara [a,*]

[a] *Department of Microbiology and Cell Biology, The Tokyo Metropolitan Institute of Medical Science, 3-18-22, Honkomagome, Bunkyo-ku, Tokyo 113-8613, Japan*
[b] *Department of Molecular Preventive Medicine, School of Medicine, The University of Tokyo, 7-3-1, Hongo, Bunkyo-ku, Tokyo 113-0033, Japan*
[c] *Department of Virology, Institute of Tropical Medicine, Nagasaki University, 1-12-4, Sakamoto, Nagasaki 852-8523, Japan*
[d] *Post Genome Institute Co., Ltd., 3-38-1, Hongo, Bunkyo-ku, Tokyo 113-0033, Japan*
[e] *Pharmaceuticals Research Unit, Research & Development Division, Mitsubishi Pharma Corporation, 1000, Kamoshida-cho, Aoba-ku, Yokohama 227-0033, Japan*
[f] *Division of Molecular Virology, Institute for Genetic Medicine, Hokkaido University, N15 W7, Kita-ku, Sapporo 060-0815, Japan*
[g] *Third Department of Virology, National Institute of Infectious Diseases, 4-7-1, Gakuen, Musashimurayama 208-0011, Japan*
[h] *Department of Virology, National Institute of Hygiene and Epidemiology, Hanoi, Vietnam*
[i] *The Chemo-Sero-Therapeutic Research Institute, 1-6-1, Okubo, Kumamoto 860-8568, Japan*

Received 15 May 2006; received in revised form 20 July 2006; accepted 19 August 2006
Available online 11 September 2006

Abstract

A vaccine for severe acute respiratory syndrome (SARS) is being intensively pursued against its re-emergence. We generated a SARS coronavirus (SARS-CoV) spike protein-expressing recombinant vaccinia virus (RVV-S) using highly attenuated strain LC16m8. Intradermal administration of RVV-S into rabbits induced neutralizing (NT) antibodies against SARS-CoV 1 week after administration and the NT titer reached 1:1000 after boost immunization with RVV-S. Significantly, NT antibodies against SARS-CoV were induced by administration of RVV-S to rabbits that had been pre-immunized with LC16m8. RVV-S can induce NT antibodies against SARS-CoV despite the presence of NT antibodies against VV. These results suggest that RVV-S may be a powerful SARS vaccine, including in patients previously immunized with the smallpox vaccine.

Keywords: SARS coronavirus; Recombinant vaccinia virus; LC16m8

1. Introduction

In November 2002, an influenza-like acute pneumonia designated as severe acute respiratory syndrome (SARS) by the World Health Organization, first emerged in China and spread to 29 countries within a few months. By July 2003, 8098 probable cases with 774 deaths were reported (www.cdc.gov/mmwr/mguide_sars.html). The etiologic agent of SARS was identified as a novel type of coronavirus (CoV) that was genetically distinct from previously characterized members of the Coronaviridae family [1–3]. Like other coronaviruses, SARS-CoV is a positive stranded RNA virus with an approximately 30 kb genome encoding non-structural proteins as well as structural proteins, including spike, envelope, membrane and nucleocapsid. Spike protein is a type I transmembrane glycoprotein that mediates binding to the host cell receptor using an amino-terminal S1

* Corresponding author. Tel.: +81 3 4463 7589; fax: +81 3 3828 8945.
E-mail address: mkohara@rinshoken.or.jp (M. Kohara).

0264-410X/$ – see front matter © 2006 Elsevier Ltd. All rights reserved.
doi:10.1016/j.vaccine.2006.08.039

domain and membrane fusion using a carboxyl-terminal S2 domain [4]. Angiotensin-converting enzyme 2 (ACE2) binds to the S1 domain of SARS-CoV spike protein and functions as a receptor for SARS-CoV [5]. CoV spike protein is a major target of protective immunity [6], and neutralizing (NT) antibodies and cytotoxic T lymphocytes against SARS-CoV spike protein have been detected in SARS patients [7,8]. These findings indicate that SARS-CoV spike protein is an appropriate target for vaccines and therapy.

The SARS epidemic broke in May 2003. However, several cases of SARS were reported in China in 2004. Although the civet cat and bats are suspected to be the natural hosts of SARS-CoV, the reservoir of SARS-CoV has yet to be identified [9–11]. In addition, the precise mechanism underlying the development of SARS is not clear and the therapeutic guidelines for SARS have not been established. It has been reported that prophylactic and therapeutic treatment with pegylated IFN-α reduces viral replication and excretion in SARS-CoV infected macaques [12]. Although pegylated IFN-α may eventually become a good therapeutic agent for SARS after infection, it cannot provide long-term protection when used as a prophylactic agent. Therefore, the development of a SARS vaccine is imperative. Several groups have reported a number of SARS vaccine candidates, including inactivated SARS-CoV vaccines [13,14], DNA vaccines [15,16] and recombinant viral vaccines [17–19] expressing one or more SARS-CoV structural proteins. Recombinant live viral vaccines can generally induce strong and long-term immunity, similar to an attenuated live vaccine, and can be abundantly manufactured in a short period of time. More importantly, a safe vaccine can be developed using an attenuated strain that has already been proven safe.

Vaccinia virus (VV) is a double stranded DNA virus with an approximately 180 kb genome, and attenuated strains have been used as the smallpox vaccine. A long DNA fragment is able to be inserted into the VV genome by homologous recombination without damaging viral integrity, as the VV genome is large and contains genes non-essential for viral replication. In fact, recombinant VV can express various proteins encoded by the transduced gene, including the glycosylated proteins of pathogens, some of which have been evaluated as candidates for prophylactic and therapeutic vaccines [20]. Lister is the attenuated VV strain that was used in the worldwide smallpox eradication program. However, additional attenuated strains were generated from Lister due to its side effects, which included erythema, fever and encephalitis. LC16m8 was isolated from Lister via the intermediate strains, LC16 and LC16mO, by multiple plaque purification in primary rabbit kidney cells. LC16m8 is characterized by temperature sensitivity and the formation of small pocks [21]. No serious side effects were observed among the over 100,000 people who were immunized with LC16m8, while the immunogenicity of LC16m8 is similar to that of Lister [22]. Therefore, LC16m8 was authorized as the vaccine against smallpox by the Japanese Ministry of Health and Welfare in 1975.

Recombinant VV expresses proteins encoded by transduced genes under the control of its own promoters. Highly efficient hybrid promoters have been developed and are composed of poxvirus A-type inclusion body (ATI) late promoter and tandem repeats of mutated 7.5 kDa protein (p7.5) early promoter [23]. The protein expressed under the control of the ATI/p7.5 hybrid promoter strongly induces both humoral and cellular immunity [24]. In the present study, we generated a recombinant VV expressing SARS-CoV spike protein (RVV-S) under the control of the ATI/p7.5 hybrid promoter, using LC16m8, and examined whether RVV-S could be used as a SARS vaccine.

2. Materials and methods

2.1. Viruses and cells

SARS-CoV (Vietnam/NB-04/2003 strain), which was isolated from nasal and throat swabs from 1 patient in Hanoi, has been previously described [25]. LC16m8 and LC16mO were kindly provided by the Chemo-Sero-Therapeutic Research Institute (Kumamoto, Japan). The RK13 cell line (ATCC: CCL-37) and VERO E6 cell line (ATCC: CRL-1586) were cultured in MEM (Nissui Pharmaceutical Co. Ltd., Tokyo, Japan) containing 5% fetal bovine serum.

2.2. Generation of recombinant vaccinia virus

The pSFJ1-10 vector contains the ATI/p7.5 hybrid promoter within the hemagglutinin (HA) gene region of VV [23]. Full length cDNA encoding the SARS-CoV spike protein gene was cloned from SARS-CoV viral RNA by RT-PCR, and then inserted downstream of the ATI/p7.5 hybrid promoter of pSFJ1-10; final designation: pSFJ1-10-SARS-S. pSFJ1-10-SARS-S was then transfected into RK13 cells that had been infected with LC16m8 at a multiplicity of infection (moi) of 10 plaque forming units (PFU)/cell. At 24 h after transfection, the virus was harvested. HA negative plaques were cloned as described previously [26]. Briefly, the harvested virus was re-infected into RK13 cells. At 96 h after infection, cells were washed with PBS (+) twice, and then incubated with chicken erythrocytes for 30 min at 30 °C. Following washing again with PBS (+), white plaques were isolated. Isolated viruses were cloned by three serial rounds of plaque purification using erythrocyte agglutination and then propagated in RK13 cells. Insertion of the SARS-CoV spike protein gene into LC16m8 genome was confirmed by direct PCR and expression was detected by Western blotting. The viral titer of RVV-S was determined using the standard plaque assay.

2.3. Western blotting

RK13 cells were infected with RVV-S or LC16m8 at moi 10. After 24 h infection, cells were lysed with RIPA

Table 1
Immunization schedule of RVV-S and LC16m8

Rabbit #	0 week		6 weeks		12 weeks		18 weeks	
	Virus	Dose (PFU)	Virus	Dose (PFU)	Virus	Dose (PFU)	Virus	Dose (PFU)
R1–R3	RVV-S	10^8	RVV-S	10^8				
R4–R6	LC16m8	10^8	LC16m8	10^8	RVV-S	10^8	RVV-S	10^8
R7–R9	RVV-S	10^6	RVV-S	10^6				
R10–R12	RVV-S	10^7	RVV-S	10^7				
R13–R15	LC16m8	10^7	RVV-S	10^7	RVV-S	10^7		

buffer (10 mM Tris, pH 7.4, 150 mM NaCl, 1% SDS and 0.5% Nonidet-P40), and 30 μg of total protein was subjected to 7.5% SDS-PAGE and was transferred to a polyvinylidene difluoride membrane (Immobilon-P, Millipore, Bedford, MA). The membrane was blocked in 5% skim milk in TBS containing 0.1% Tween-20 (TBS-T) and then washed with TBS-T. Polyclonal antibodies against spike protein were used as the primary antibody. These were prepared from rabbit sera immunized with a KLH-conjugated spike protein peptide (amino acid residues 559–570 or 1236–1248) and the IgG fraction purified using the Ampure PA kit (Amersham Bioscience, Piscataway, NJ). Antigen-antibody interaction was detected by horseradish peroxidase (HRP)-conjugated donkey anti-rabbit polyclonal antibodies (Amersham Bioscience) and visualized using the ECL system (Amersham Bioscience).

2.4. Immunofluorescence analysis

RK13 cells seeded on slide-glass were infected with RVV-S or LC16m8 at moi 5. At 12 h after incubation at 30 °C, cells were fixed in cold acetone/methanol and then blocked in 1% BSA in PBS (−) for 1 h at room temperature. Following removal of the blocking buffer, cells were incubated with polyclonal antibodies against spike protein, which recognize the C-terminal peptide of spike protein (amino acid residues 1236–1248), for 1 h at room temperature. Following three washes with PBS containing 0.05% Tween-20 (PBS-T), cells were incubated with Alexa 488-conjugated anti-rabbit IgG (Invitrogen, Carlsbad, CA) for 1 h at room temperature. After washing again with PBS-T, the slide-glasses were mounted in Permafluor (Beckman Coulter, Fullerton, CA) containing 1 μg/ml 6-diamidino-2-phenylindole (DAPI) and analyzed using a confocal microscope (LSM510, Carl Zeiss, Oberkochen, Germany).

2.5. Immunization of rabbits

Groups of three New Zealand White rabbits, which were purchased from SLC (Hamamatsu, Japan), were intradermally immunized with one of several doses (10^6, 10^7 or 10^8 PFU) of RVV-S, or with 10^8 PFU of LC16m8, at 0 and 6 weeks. The LC16m8 immunized group was further immunized with 10^8 PFU of RVV-S at 12 and 18 weeks. Another group of three rabbits was immunized with 10^7 PFU of LC16m8 at 0 week, and then immunized with 10^7 PFU of RVV-S at 6 and 12 weeks. A summary of the immunization schedule is shown in Table 1. Sera were collected every week, and used for enzyme linked immunosorbent assay (ELISA) and the *in vitro* neutralization (NT) assay below. All animal experiments were approved by The Tokyo Metropolitan Institute of Medical Science Animal Experiment Committee and were performed in accordance with the animal experimentation guidelines of The Tokyo Metropolitan Institute of Medical Science.

2.6. ELISA

Full length recombinant SARS-CoV spike protein containing a six-histidine tag (His) was expressed in RK13 cells by RVV-S-His, which was generated from LC16mO, and purified using Nickel sepharose (Amersham Bioscience). Peptides from the N-terminal (mixture of three peptides, amino acid residues 12–53, 90–115 and 171–203), middle position (mixture of two peptides, amino acid residues 408–470 and 540–573) and C-terminal (mixture of three peptides, amino acid residues 1051–1076, 1121–1154 and 1162–1190) of the spike protein, which respond to sera from SARS-infected individuals, were purchased from ProSpec-Tany TechnoGene Ltd. (Rehovot, Israel). These three peptide mixtures or full length spike protein were coated onto the 96 well plates at 4 °C. The plates were blocked with 1% BSA in PBS (−) containing 0.5% Tween-20 and 2.5 mM EDTA, and then incubated with serial dilutions of sera from the rabbits immunized with RVV-S or LC16m8. After extensive washing, the plates were incubated with HRP-conjugated donkey anti-rabbit polyclonal antibodies (Amersham Bioscience). Antigen–antibody interactions were detected using 3,3′,5,5′-tetramethylbenzidine solution as the substrate (Becton Dickinson, San Jose, CA), and the binding activity was measured by the absorbance at 450 nm.

2.7. In vitro NT assay for SARS-CoV

Serial dilutions of heat-inactivated sera were mixed with equal volumes of 100 $TCID_{50}$ of SARS-CoV and incubated at 37 °C for 1 h. VERO E6 cells were then infected with the virus/sera mixtures in 96 well plates. At 120 h after infection, the NT titer was determined as the maximum dilution of sera that inhibited the SARS-CoV induced cytopathic effect by more than 50%. All experiments with SARS-CoV were performed in a biosafety containment level III facility.

2.8. In vitro NT assay for VV

Serial dilutions of heat-inactivated sera were mixed with equal volumes of 100 PFU of LC16mO, and incubated at 37 °C for 1 h, followed by incubation at 4 °C for 16 h. RK13 cells were then infected with the virus/sera mixtures in 6 well plates. At 48 h after infection, the NT titer was determined as the maximum dilution of sera that inhibited plaque formation by more than 50%.

2.9. Statistical analysis

All data were expressed as mean ± S.E.M. Data for RVV-S dose dependent effect were statistically analyzed by one-way ANOVA followed by Turkey test. Data for LC16m8 pre-immunization effect were statistically analyzed by Student's or by Welch's t-test. $p < 0.05$ was considered to be statistically significant.

3. Results

3.1. Generation and characterization of RVV-S

The full length SARS-CoV spike protein gene was inserted by homologous recombination into the HA gene region of LC16m8, which was located downstream of the powerful ATI/p7.5 hybrid promoter (Fig. 1A). Recombination between pSFJ1-10-SARS-S and LC16m8 results in inactivation of the HA gene. We screened for RVV-S using the erythrocyte agglutination assay, and insertion of the transduced gene was then confirmed by PCR. To confirm the expression of SARS-CoV spike protein, Western blotting was performed. Two kinds of rabbit polyclonal antibodies that recognized different epitopes, amino acid residues 559–570 and 1236–1248 of SARS-CoV spike protein, were used as the primary antibody. In RVV-S but not LC16m8 infected cells, both antibodies detected an approximately 180 kDa protein (Fig. 1B and C), which is consistent with the molecular mass of spike protein [18]. SARS-CoV spike protein is reported to be highly glycosylated, and thus the molecular mass on SDS-PAGE is larger than that predicted from the gene sequence [18]. Expression of spike protein following infection with RVV-S was also confirmed by immunofluorescence analysis. RVV-S infected VERO E6 cells were stained with antibody against spike protein, whereas no staining was observed in the cells infected with LC16m8 or the uninfected control cells (Fig. 1D).

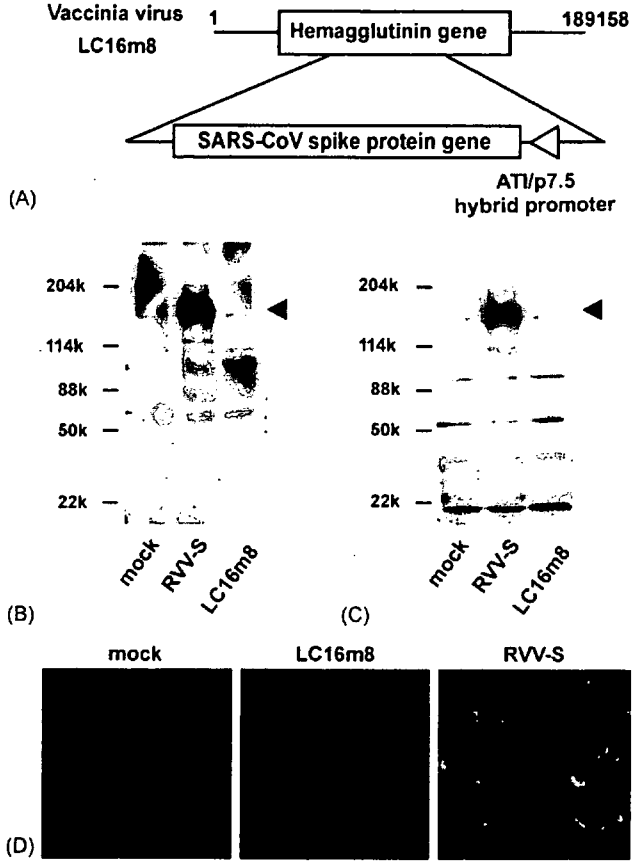

Fig. 1. Characteristics of SARS-CoV spike protein-expressing recombinant vaccinia virus (RVV-S) derived from LC16m8. (A) The full length SARS-CoV spike protein gene was inserted into the HA gene region of the LC16m8 genome. The ATI/p7.5 hybrid promoter regulates expression of spike protein. (B and C) RK13 cells were infected with RVV-S or LC16m8 at moi 10. At 24 h after infection, cells were harvested and analyzed. Two kinds of anti-SARS-CoV spike protein polyclonal antibodies, which recognize different epitopes, namely amino acid residues 559–570 (B) and 1236–1248 (C) of spike protein, were used as the primary antibodies. The molecular masses of marker proteins in kDa are shown on the left and the position of the spike protein is indicated by an arrowhead on the right. (D) Indirect immunofluorescence staining of spike protein. Expression of spike protein was visualized by staining with anti-SARS-CoV spike polyclonal antibodies, followed by Alexa 488-conjugated anti-rabbit IgG (green). Nuclei were stained with DAPI (red).

3.2. Induction of binding antibodies against spike protein in RVV-S-immunized rabbits

To investigate whether RVV-S induces binding antibodies against spike protein, 10^8 PFU of RVV-S or LC16m8 (as the control) was intradermally injected into rabbits at 0 and 6 weeks. Rabbits immunized with either RVV-S or LC16m8 did not exhibit weight loss or any clinical signs except for regional skin reactions, such as erythema and induration. The skin reaction induced by RVV-S was comparable to that induced by LC16m8 (data not shown). Binding antibodies against full length spike protein were detected by ELISA in the sera from rabbits immunized with RVV-S (Fig. 2A). Next, we investigated the binding activities of immunized sera against different epitopes of the spike protein. RVV-S-immunized sera reacted with all three regions of spike protein. The sera bound to the C-terminal peptides, which contained the heptad repeat 2 (HR2) region, reported to be the NT epitope of SARS-CoV (Fig. 2B) [27] and to the middle peptides,

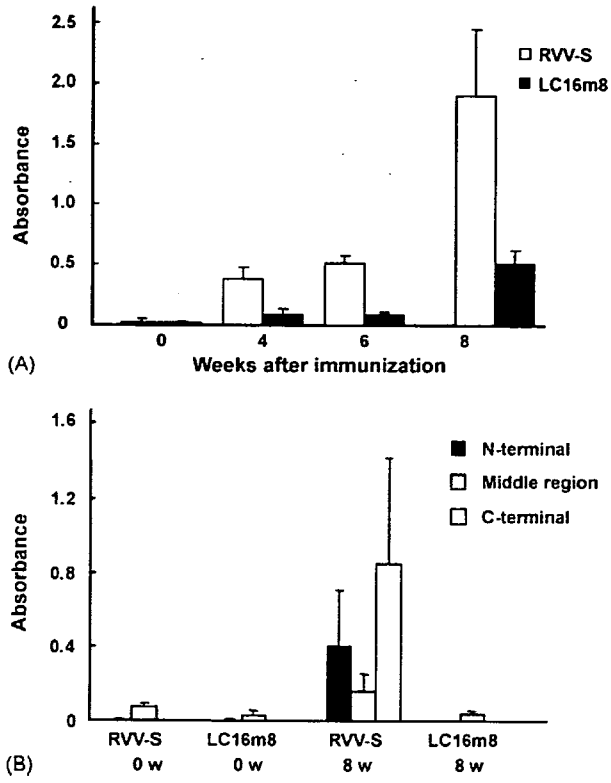

Fig. 2. Induction of binding antibodies against SASR-CoV spike protein. New Zealand White rabbits ($n = 3$) were immunized with 10^8 PFU of RVV-S (R1-3; open symbols) or LC16m8 (R4–6; closed symbols) at 0 and 6 weeks. The binding activity of 10^3- or 10^4-fold dilutions of immunized sera was assessed using His-tagged full length spike protein (A), or one of three kinds of spike protein partial peptides (B), as the capture antigen.

in which a receptor binding domain, another NT epitope of SARS-CoV, was included [28].

3.3. Induction of NT antibodies against SARS-CoV in RVV-S-immunized rabbits

Next, to determine whether the antibodies induced by immunization with RVV-S have NT activity against SARS-CoV, we performed an *in vitro* NT assay against SARS-CoV using immunized sera. Interestingly, the sera obtained from all three rabbits in this group showed NT activity against SARS-CoV, even at 1 week after immunization with 10^8 PFU of RVV-S (Fig. 3A). The NT titer reached 1:100 at 3 weeks, and increased 10-fold further by boost immunization. In contrast, sera obtained from rabbits immunized with LC16m8 did not show any NT activity against SARS-CoV (Fig. 3A). Next, to determine the minimum dose that can induce NT antibodies against SARS-CoV by single immunization, rabbits were immunized with lower doses of RVV-S. All three rabbits that underwent single immunization with 10^7 PFU of RVV-S generated NT antibodies against SARS-CoV (Fig. 3A). The NT titer further increased by boost immunization with 10^7 PFU of RVV-S and reached a comparable level to that induced by 10^8 PFU of RVV-S (Fig. 3B). On the other hand, NT activity was induced by single immunization with 10^6 PFU of RVV-S at 2 and 4 weeks after immunization in all three rabbits, but then decreased below the detection limit in one rabbit at 6 weeks (Fig. 3A). However, the NT titer increased to approximately 1:300 in the group immunized with 10^6 PFU of RVV-S by boost immunization with the same dose of RVV-S (Fig. 3B).

3.4. RVV-S induces NT antibodies against SARS-CoV in the presence of NT antibodies against VV

Induction of NT antibodies against VV by RVV-S was next examined. The *in vitro* NT assay against VV revealed that LC16m8 and RVV-S equally induced NT antibodies against VV in the rabbits (Fig. 3C). NT activity against VV was induced by 10^8 PFU of RVV-S at 1 week after immunization, similar to SARS-CoV. The NT titer against VV, which reached 1:10,000 at 2 weeks after boost immunization with 10^8 PFU of RVV-S, was similar to that induced by 10^8 PFU of LC16m8. These results suggest that the epitopes of the NT antibodies against VV were preserved in RVV-S. Since VV has been used as a smallpox vaccine in humans, we were concerned that RVV-S might be eliminated by the host's immune response before inducing effective immunity against a protein encoded by the transduced gene. Therefore, to assess whether RVV-S can induce NT antibodies against SARS-CoV in rabbits that had NT antibodies against VV, RVV-S was injected into rabbits which had been pre-immunized with LC16m8. NT antibodies against VV were induced in the rabbits by single immunization with 10^7 PFU of LC16m8 and the NT titer reached 1:64–256 (Fig. 4A). By following immunization with an equal dose of RVV-S (10^7 PFU), NT antibodies against SARS-CoV were induced in all three rabbits, although induction of NT antibodies was delayed in one rabbit (R14). Although the induction of NT antibodies against SARS-CoV was partially suppressed in the LC16m8 pre-immunized rabbits, the NT titer further increased in all three rabbits by boost immunization with RVV-S (Fig. 4C). These results suggest that RVV-S can induce NT antibodies in individuals who have been previously immunized with a smallpox vaccine. Next, we examined whether RVV-S induced NT antibodies against SARS-CoV in rabbits with a high titer of NT antibodies against VV. The NT titer against VV in rabbits that had been immunized twice with 10^8 PFU of LC16m8 was sustained at approximately 1:4000 (Fig. 4B). Although these rabbits had an extremely high titer of NT antibodies against VV, NT antibodies against SARS-CoV were induced in all three rabbits upon a booster injection with 10^8 PFU of RVV-S (Fig. 4B). Surprisingly, the NT titer of these rabbits increased to levels comparable to those of the non-pre-immunized rabbits (Fig. 4C). These results indicate that an immune response against a protein encoded by a transduced gene can be induced by immunization with 10^8 PFU of RVV in spite of the pre-existence of NT antibodies against VV.

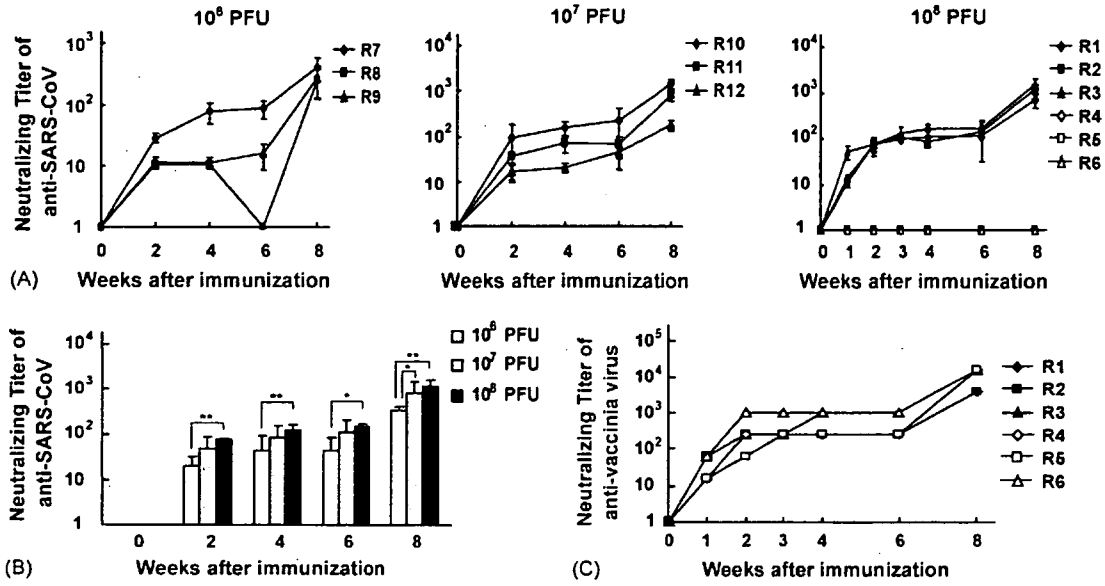

Fig. 3. Induction of NT antibodies against SARS-CoV and vaccinia virus. (A) The NT activity against SARS-CoV of RVV-S- (10^6 PFU, R7–9; 10^7 PFU, R10–12; 10^8 PFU, R1–3; closed symbols) or 10^8 PFU of LC16m8- (R4–6; open symbols) immunized rabbit sera was defined as the maximum dilution of sera that inhibited the cytopathic effect of SARS-CoV by more than 50%. (B) The dose dependency of immunization with RVV-S shown in (A). $^{*}p<0.05$, $^{**}p<0.01$. (C) The NT activity against vaccinia virus of RVV-S- (R1–3, closed symbols) or LC16m8- (R4–6, open symbols) immunized sera was defined as the maximum dilution of sera that inhibited plaque formation by LC16mO by more than 50%.

4. Discussion

In the present study, we generated a SARS-CoV spike protein-expressing recombinant vaccinia virus using a highly attenuated strain, LC16m8, and demonstrated that NT antibodies against SARS-CoV can be strongly induced by immunization with RVV-S, not only in naïve rabbits but also in LC16m8 pre-immunized rabbits.

In a previous study, passive transfer of sera obtained from mice inoculated with SARS-CoV prevented the replication of SARS-CoV in the upper and lower respiratory tract [29]. In addition, intraperitoneal injection of sera from mice immunized with MVA expressing spike protein (MVA/S) reduced the viral titers in lung and nasal turbinate in a dose-dependent manner [18]. These finding indicate that NT antibodies against spike protein are sufficient to protect against SARS-CoV infection. Single immunization with 10^7 or 10^8 PFU of RVV-S and two immunizations with 10^6 PFU of RVV-S were able to induce a high level of NT antibodies against SARS-CoV at 2 weeks after immunization. Therefore, RVV-S also may protect against SARS-CoV *in vivo* and would be a highly effective vaccine against SARS in naïve individuals.

Contrary to the above studies [18,29], Czub et al. [30] reported that immunization with MVA/S did not prevent SARS-CoV infection in ferrets but rather produced inflammatory responses and focal necrosis in the liver after SARS-CoV challenge. This may have been due to only low NT activity against SARS-CoV being induced by the MVA/S immunization. Moreover, the precise mechanism of this liver inflammation has not been clarified. Feline infectious peritonitis virus (FIPV), another member of the coronaviruses, exhibited enhanced FIPV infection into monocytes/macrophages through viral-specific antibody binding to the Fc receptors of these cells, and caused enhanced inflammation [31]. However, there is no evidence that NT antibodies against SARS-CoV cause antibody-dependent enhancement, and correlation between inflammation and antibody-dependent enhancement by MVA/S vaccination has not yet been established. The side effects of vaccines are also influenced by the dosage and route of immunization. In Czub's report, MVA/S was intraperitoneally injected into the ferrets, although most vaccinations with RVV are conducted through other routes, such as intradermal, intramuscular or subcutaneous injection. Therefore, selection of a different immunization route may prevent such side effects. Nonetheless, further analysis of the side effects of various SARS vaccines, including RVV-S, is required in *in vivo* SARS-CoV challenge models in a variety of animals.

Using RVV-S as a candidate SARS vaccine means that possible complications due to previous vaccination with the VV for smallpox may be avoided. Hammarlund et al. [32] reported that a particular antiviral antibody against poxvirus is maintained for a very long time (possibly for life) by immunization with the smallpox vaccine. Therefore, there was concern that a RVV vaccine would be eliminated by the host antiviral immune response before induction of effective humoral and/or cellular immunity against the protein encoded by the transduced gene. However, immunization with 10^7 PFU of RVV-S induced NT antibodies against SARS-CoV in rabbits that had been immunized with 10^7 PFU

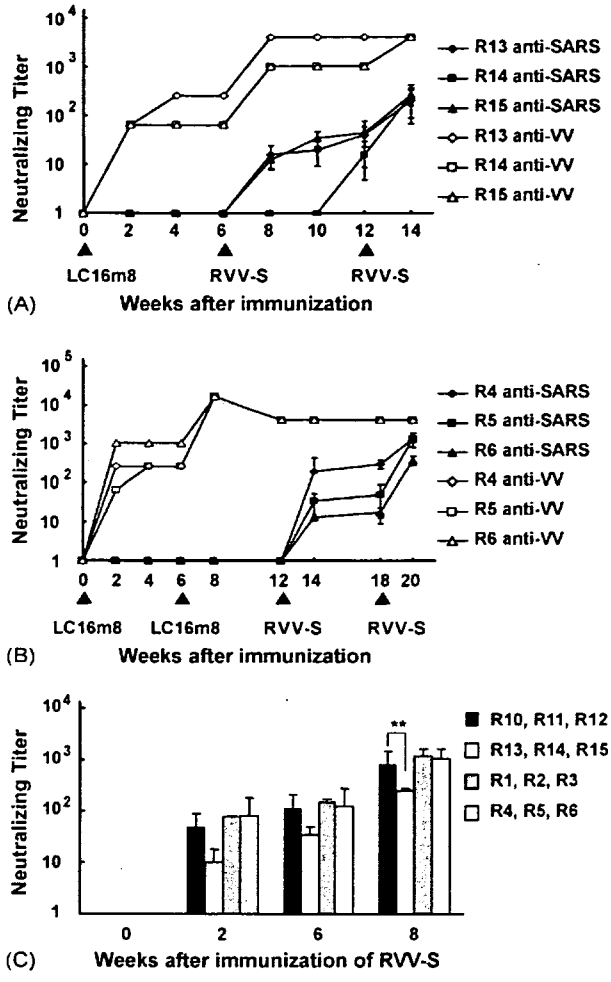

Fig. 4. Induction of NT antibodies against SARS-CoV in rabbits pre-immunized with LC16m8. (A) Three rabbits (R13–15) were immunized with 10^7 PFU of LC16m8 on day 0, and then immunized with 10^7 PFU of RVV-S at 6 and 12 weeks. (B) Three rabbits (R4–6) were immunized with 10^8 PFU of LC16m8 at 0 and 6 weeks, and then immunized with 10^8 PFU of RVV-S at 12 and 18 weeks. Immunized rabbit sera were analyzed by *in vitro* NT assay against SARS-CoV (closed symbols) or vaccinia virus (open symbols). Each type of symbol indicates one and the same individual, and the schedule of immunization with RVV-S or LC16m8 is indicated by arrowheads. (C) Comparison of NT antibodies against SARS-CoV induced by RVV-S in VV-immunized or naïve rabbits. RVV-S (10^7 or 10^8 PFU) was injected into rabbits at 0 and 6 weeks in the presence (10^7 PFU, R13–15; 10^8 PFU, R4–6) or absence (10^7 PFU, R10–12; 10^8 PFU, R1–3) of pre-immunization with an equal titer of LC16m8. Immunized rabbit sera were analyzed by *in vitro* NT assay against SARS-CoV. $^{**}p < 0.01$.

of LC16m8. Since the NT titer against VV induced by 10^7 PFU of LC16m8 was comparable to that in people vaccinated with the smallpox vaccine [32], RVV-S may induce NT antibodies against SARS-CoV in such people. On the other hand, 10^8 PFU of RVV-S also induced NT antibodies against SARS-CoV in rabbits that had an extremely high titer of NT antibodies against VV due to two pre-immunizations with 10^8 PFU of LC16m8. Furthermore, there was no difference in the NT titer against SARS-CoV induced by RVV-S between naïve rabbits and LC16m8 pre-immunized rabbits. The immune response against a protein encoded by a transduced gene may be influenced by the amount of antigen expression, the antigenicity of the protein encoded by a transduced gene, the route of immunization and viral proliferation in the host, and thus further analysis is required to resolve the precise mechanism involved. Furthermore, the vaccine effect of RVV-S still needs to be confirmed in humans pre-immunized with the smallpox vaccine.

In the present study, immunization with RVV-S manifested a vaccine effect against SARS-CoV, in spite of the pre-existing NT antibodies against VV. This finding indicates that an RVV vaccine derived from LC16m8 can be used for people previously immunized with the smallpox vaccine. Furthermore, this RVV vaccine could be repeatedly used against various microbes, such as influenza virus, by alteration of the protein encoded by the transduced gene. Therefore, the use of an RVV vaccine generated from LC16m8 is a promising vaccine strategy against various infectious diseases.

Acknowledgments

We thank Y. Sameshima for technical assistance with generation of the recombinant vaccinia virus. We are very grateful to Dr. M. Shuda for helpful discussion. We also thank S. Morikawa of the Department of Virology, National Institute of Infectious Diseases, Tokyo, Japan, for kindly providing the SARS-CoV immunized rabbit sera. This study was supported in part by a Grant for Research on Emerging and Re-emerging Infectious Diseases from the Ministry of Health, Labor and Welfare, Japan, the 21st Century Centers of Excellence [COE] program on Global strategies for Control of Tropical and Emerging Infectious Diseases at Nagasaki University, and the Ministry of Education, Culture, Sports, Science and Technology of Japan.

References

[1] Drosten C, Gunther S, Preiser W, van der Werf S, Brodt HR, Becker S, et al. Identification of a novel coronavirus in patients with severe acute respiratory syndrome. N Engl J Med 2003;348(20):1967–76.
[2] Ksiazek TG, Erdman D, Goldsmith CS, Zaki SR, Peret T, Emery S, et al. A novel coronavirus associated with severe acute respiratory syndrome. N Engl J Med 2003;348(20):1953–66.
[3] Peiris JS, Lai ST, Poon LL, Guan Y, Yam LY, Lim W, et al. Coronavirus as a possible cause of severe acute respiratory syndrome. Lancet 2003;361(9366):1319–25.
[4] Gallagher TM, Buchmeier MJ. Coronavirus spike proteins in viral entry and pathogenesis. Virology 2001;279(2):371–4.
[5] Li W, Moore MJ, Vasilieva N, Sui J, Wong SK, Berne MA, et al. Angiotensin-converting enzyme 2 is a functional receptor for the SARS coronavirus. Nature 2003;426(6965):450–4.
[6] Spaan W, Cavanagh D, Horzinek MC. Coronaviruses: structure and genome expression. J Gen Virol 1988;69(Pt. 12):2939–52.
[7] Nie Y, Wang G, Shi X, Zhang H, Qiu Y, He Z, et al. Neutralizing antibodies in patients with severe acute respiratory syndrome-associated coronavirus infection. J Infect Dis 2004;190(6):1119–26.

[8] Wang YD, Sin WY, Xu GB, Yang HH, Wong TY, Pang XW, et al. T-cell epitopes in severe acute respiratory syndrome (SARS) coronavirus spike protein elicit a specific T-cell immune response in patients who recover from SARS. J Virol 2004;78(11):5612–8.
[9] Normile D, Enserink M. SARS in China. Tracking the roots of a killer. Science 2003;301(5631):297–9.
[10] Li W, Shi Z, Yu M, Ren W, Smith C, Epstein JH, et al. Bats are natural reservoirs of SARS-like coronaviruses. Science 2005;310(5748):676–9.
[11] Lau SK, Woo PC, Li KS, Huang Y, Tsoi HW, Wong BH, et al. Severe acute respiratory syndrome coronavirus-like virus in Chinese horseshoe bats. Proc Natl Acad Sci USA 2005;102(39):14040–5.
[12] Haagmans BL, Kuiken T, Martina BE, Fouchier RA, Rimmelzwaan GF, van Amerongen G, et al. Pegylated interferon-alpha protects type 1 pneumocytes against SARS coronavirus infection in macaques. Nat Med 2004;10(3):290–3.
[13] Tang L, Zhu Q, Qin E, Yu M, Ding Z, Shi H, et al. Inactivated SARS-CoV vaccine prepared from whole virus induces a high level of neutralizing antibodies in BALB/c mice. DNA Cell Biol 2004;23(6):391–4.
[14] Takasuka N, Fujii H, Takahashi Y, Kasai M, Morikawa S, Itamura S, et al. A subcutaneously injected UV-inactivated SARS coronavirus vaccine elicits systemic humoral immunity in mice. Int Immunol 2004;16(10):1423–30.
[15] Yang ZY, Kong WP, Huang Y, Roberts A, Murphy BR, Subbarao K, et al. A DNA vaccine induces SARS coronavirus neutralization and protective immunity in mice. Nature 2004;428(6982):561–4.
[16] Kim TW, Lee JH, Hung CF, Peng S, Roden R, Wang MC, et al. Generation and characterization of DNA vaccines targeting the nucleocapsid protein of severe acute respiratory syndrome coronavirus. J Virol 2004;78(9):4638–45.
[17] Gao W, Tamin A, Soloff A, D'Aiuto L, Nwanegbo E, Robbins PD, et al. Effects of a SARS-associated coronavirus vaccine in monkeys. Lancet 2003;362(9399):1895–6.
[18] Bisht H, Roberts A, Vogel L, Bukreyev A, Collins PL, Murphy BR, et al. Severe acute respiratory syndrome coronavirus spike protein expressed by attenuated vaccinia virus protectively immunizes mice. Proc Natl Acad Sci USA 2004;101(17):6641–6.
[19] Buchholz UJ, Bukreyev A, Yang L, Lamirande EW, Murphy BR, Subbarao K, et al. Contributions of the structural proteins of severe acute respiratory syndrome coronavirus to protective immunity. Proc Natl Acad Sci USA 2004;101(26):9804–9.
[20] Moss B. Genetically engineered poxviruses for recombinant gene expression, vaccination, and safety. Proc Natl Acad Sci USA 1996;93(21):11341–8.
[21] Sugimoto M, Yasuda A, Miki K, Morita M, Suzuki K, Uchida N, et al. Gene structures of low-neurovirulent vaccinia virus LC16m0, LC16m8, and their Lister original (LO) strains. Microbiol Immunol 1985;29(5):421–8.
[22] Yamaguchi M, Kimura M, Hirayama M. Report of the National Smallpox Vaccination Research Committee: study of side effects, complications and their treatments. Clin Virol 1975;3:269–78.
[23] Jin NY, Funahashi S, Shida H. Constructions of vaccinia virus A-type inclusion body protein, tandemly repeated mutant 7.5 kDa protein, and hemagglutinin gene promoters support high levels of expression. Arch Virol 1994;138(3–4):315–30.
[24] Funahashi S, Itamura S, Iinuma H, Nerome K, Sugimoto M, Shida H. Increased expression in vivo and in vitro of foreign genes directed by A-type inclusion body hybrid promoters in recombinant vaccinia viruses. J Virol 1991;65(10):5584–8.
[25] Hong TC, Mai QL, Cuong DV, Parida M, Minekawa H, Notomi T, et al. Development and evaluation of a novel loop-mediated isothermal amplification method for rapid detection of severe acute respiratory syndrome coronavirus. J Clin Microbiol 2004;42(5):1956–61.
[26] Shida H, Tochikura T, Sato T, Konno T, Hirayoshi K, Seki M, et al. Effect of the recombinant vaccinia viruses that express HTLV-I envelope gene on HTLV-I infection. Embo J 1987;6(11):3379–84.
[27] Keng CT, Zhang A, Shen S, Lip KM, Fielding BC, Tan TH, et al. Amino acids 1055 to 1192 in the S2 region of severe acute respiratory syndrome coronavirus S protein induce neutralizing antibodies: implications for the development of vaccines and antiviral agents. J Virol 2005;79(6):3289–96.
[28] Chen Z, Zhang L, Qin C, Ba L, Yi CE, Zhang F, et al. Recombinant modified vaccinia virus Ankara expressing the spike glycoprotein of severe acute respiratory syndrome coronavirus induces protective neutralizing antibodies primarily targeting the receptor binding region. J Virol 2005;79(5):2678–88.
[29] Subbarao K, McAuliffe J, Vogel L, Fahle G, Fischer S, Tatti K, et al. Prior infection and passive transfer of neutralizing antibody prevent replication of severe acute respiratory syndrome coronavirus in the respiratory tract of mice. J Virol 2004;78(7):3572–7.
[30] Czub M, Weingartl H, Czub S, He R, Cao J. Evaluation of modified vaccinia virus Ankara based recombinant SARS vaccine in ferrets. Vaccine 2005;23(17–18):2273–9.
[31] Olsen CW, Corapi WV, Ngichabe CK, Baines JD, Scott FW. Monoclonal antibodies to the spike protein of feline infectious peritonitis virus mediate antibody-dependent enhancement of infection of feline macrophages. J Virol 1992;66(2):956–65.
[32] Hammarlund E, Lewis MW, Hansen SG, Strelow LI, Nelson JA, Sexton GJ, et al. Duration of antiviral immunity after smallpox vaccination. Nat Med 2003;9(9):1131–7.

Available online at www.sciencedirect.com
ScienceDirect
ELSEVIER
Biochemical and Biophysical Research Communications xxx (2008) xxx–xxx
BBRC
www.elsevier.com/locate/ybbrc

Nonhuman primate intestinal villous M-like cells: An effective poliovirus entry site ☆

Yoshihiro Takahashi [a,b], Shogo Misumi [b], Atsunobu Muneoka [a], Mitsuaki Masuyama [a,b], Hiroshi Tokado [a], Koichiro Fukuzaki [a], Nobutoki Takamune [b], Shozo Shoji [b,*]

[a] *Shin Nippon Biomedical Laboratories, Ltd., 2438 Miyanoura, Kagoshima 891-1394, Japan*
[b] *Department of Pharmaceutical Biochemistry, Faculty of Medical and Pharmaceutical Sciences, Kumamoto University, 5-1 Oe-Honmachi, Kumamoto 862-0973, Japan*

Received 11 January 2008

Abstract

Humans and some Old World monkeys, chimpanzees, and cynomolgus macaques, are susceptible to oral poliovirus (PV) infection. Interestingly, rhesus macaques, although sensitive to injected PV, are not susceptible to gut infection. Not much is known about the initial event of gut infection by PV in rhesus macaques so far. Here, we show that PV can efficiently enter the lamina propria (LP) by penetrating across intestinal villous M-like cells in rhesus macaques. We found by immunofluorescence analysis that PV effectively invades LP rather than germinal centers (GCs) in rhesus macaques despite expressing PV receptor CD155 on cells within GCs and LP. Furthermore, energy dispersive X-ray spectroscopy demonstrated that gold-labeled PV is spatiotemporally internalized into villous M-like cells and engulfed by macrophage-like cells in LP. These results suggest that rhesus macaques may be resistant to productive gut PV infection owing to a defective translocation of PV to GCs.

Keywords: Villous M-like cell; Mucosa; Old World monkeys; Poliovirus; Gut infection

Nonhuman primates are the closest evolutionary relatives of humans. Their underlying physiology and metabolism, as well as genomic structure, are more similar to those in humans than to those in other mammals. This makes nonhuman primates particularly important as models of human diseases, including viral infectious diseases. Although chimpanzees are the animals most similar to humans, they are unsuitable for preclinical studies on ethical grounds because they are an endangered or threatened species. For other primates, there are the requirements of research utility and availability. Because of this, the rhesus and cynomolgus macaques are the excellent choice for pathophysiological and preclinical studies.

Humans are the only known natural hosts of poliovirus (PV), which causes poliomyelitis. In humans, PV has been isolated from tonsillopharyngeal tissues, the wall of the ileum, and mesenteric lymph nodes [1]. Oral PV infection can be associated with extensive tissue destruction in lymphoid organs of the pharynx, including the tonsils, and the small intestine, including Peyer's patches (PPs) [2], suggesting that the virus replicates in these tissues. In contrast, nonhuman primates are highly susceptible to PV via all routes except the oral route, yet some species show a certain degree of oral susceptibility [3]. Cynomolgus macaques are susceptible to infection via the oral route but only when a large dose of PV is administered. On the other hand, rhesus macaques are rarely susceptible to PV administered

Abbreviations: $CCID_{50}$, 50% cell culture infective doses; EDS, energy dispersive X-ray spectroscopy; FAE, follicle-associated epithelium; GCs, germinal centers; IFNAR, alpha/beta interferon receptor; LP, lamina propria; PV, poliovirus.

☆ The Ministry of Education, Culture, Sports, Science and Technology of Japan (16017287), and a Health Science Research Grant from the Ministry of Health, Labour, and Welfare of Japan (18220501).

* Corresponding author. Fax: +81 96 362 7800.
E-mail address: shoji@gpo.kumamoto-u.ac.jp (S. Shoji).

0006-291X/$ - see front matter
doi:10.1016/j.bbrc.2008.01.120

orally. Iwasaki et al. suggested that in rhesus macaques, CD155 expression levels are low in the follicle-associated epithelium (FAE) and CD155 is not present in GCs [4]. In contrast, in humans, CD155 was detected on the intestinal epithelium, on M cells in PPs, and in GCs within PPs [4]. These findings suggest that PV replication in the gut may depend on the presence of CD155 in FAE, including M cells, and on cells in PPs. However, the gut infection pattern of PV using rhesus macaque models has not been performed so far.

CD155 transgenic (Tg) mice are also not susceptible to oral infection by PV [5,6]. CD155 is present at very low levels in the intestinal epithelium of these mice and absent in PPs [4,7]. Overexpression of CD155 in the intestinal epithelium of Tg mice induced by a fatty acid binding protein promoter also does not lead to oral susceptibility to PV [7]. Recently, Ohka et al. [8] detected PV in the epithelia of the small intestine, which proliferated in the alimentary tract of CD155 Tg mice lacking the alpha/beta interferon receptor (IFNAR) gene. These results suggest that IFNAR plays an important role in determining permissivity in addition to the appropriate expression of CD155 in the alimentary tract of Tg mice. However, this still has not explained why healthy humans and limited Old World monkeys are highly susceptible to gut PV infection despite robust innate immune responses including interferon signaling.

Whether human epithelial or immune cells are the primary sites of PV replication in the intestinal mucosa has remained unclarified as well. Although PV may easily gain access to the surface of FAE because it remains largely free from secretions such as mucus, glycocalyx or IgA, enterocytes other than those in the FAE may not be su ciently accessible to PV to initiate infection. Furthermore, Iwasaki et al. indicated that the distribution of CD155 on human FAE-enterocytes other than M cells may not be favorable for intestinal PV infection because the distribution is higher on the basal side [4]. This notion is supported by the finding that M cells in humans are the site of PV penetration of the intestinal epithelial barrier [9]. From these results, we speculate that PV may not be preferentially absorbed into GCs through rhesus FAE-M cells and replicates in rhesus lymphoid tissues.

Typical FAE-M cells, characterized by an irregular brush border and a reduced amount of glycocalyx, e - ciently take up and transport a wide variety of macromolecules and microorganisms from the gut lumen into PPs [10–14]. A recent study demonstrated that intestinal villous M cells serve as another antigen gateway in mice for the sampling of gut bacteria and subsequent induction of Ag-specific immune responses in a PPs-independent manner [15]. Thus, it is possible that villous M cells also serve as the PV entry site in the mucosal epithelium and are involved in oral PV infection in human and some Old World monkeys.

In this study, we discovered that, in rhesus macaques, PV can penetrate into LP via intestinal villous M-like cells rather than FAE-M cells, suggesting that rhesus macaques may be resistant to gut PV infection due to a defective translocation of PV to GCs via FAE-M cells.

Materials and methods

Animals and tissue samples. Purpose-bred female rhesus macaques (*Macaca mulatta*) obtained from a supplier in China (10–12 years old, weighing 4.55–6.26 kg) were used for this study. PPs of cynomolgus macaques (weighing 5–6 kg) were obtained from 4 to 5 years old female monkeys. This study (the Permission No. 19–137) was approved and carried out according to the guidelines of the Animal Care and Use Committee of Kumamoto University.

Gold labeling of PV. PV was labeled with gold colloid solution (5 nm, British BioCell International, Ltd.) according to the instruction manual. Gold nanoparticles not anchored on PV were readily removed by centrifugation. Gold-labeled PV was subjected to negative staining electron microscopy.

Inoculation of PV. Rhesus macaques were fasted overnight. They were then inoculated with 1 ml of PV solution (type 1, $10^{5.5}$–$10^{6.5}$ 50% cell culture infective doses ($CCID_{50}$); type II, $10^{4.5}$–$10^{5.5}$ $CCID_{50}$; type III, $10^{5.0}$–$10^{6.0}$ $CCID_{50}$) or 1 ml of gold-labeled PV at a site in the ileum (15 cm from the cecum) after celiotomy under anesthesia induced by a subcutaneous injection of urethane (ethyl carbamate, 800 mg/mL; 1.5 mL/kg body weight; Wako Pure Chemical Industries, Ltd.) solution and an intravenous injection of alpha-chloralose (Wako Pure Chemical Industries, Ltd.; 20 mg/mL; 5.5 mL/kg body weight) into the cephalic vein.

Collection of PPs. The rhesus monkeys were euthanized by exsanguination under anesthesia, and the part of the ileum (15 cm from cecum) including the inoculation site was collected. After washing the collected part of the ileum, 2 cm^2 blocks of PPs were fixed in ice-cold 3% glutaraldehyde/0.1 M sucrose/phosphate-bu ered saline (pH 7.4). After 30 min of fixing, PPs were kept at 4 C.

Histopathological study. Tissue samples were fixed in 10% neutral bu ered formalin and were trimmed, embedded in para n, sectioned, stained with hematoxylin–eosin and examined by light microscopy.

Immunofluorescence staining. To examine the distribution of CD155 expression, the frozen sections of PPs were stained with various antibodies. In brief, 5 μm frozen sections were fixed in cold acetone and blocked with 1% nonfat skim milk in PBS( ). CD155 was detected using mAb D171 (Abcam Inc.) and FITC-conjugated anti-mouse IgG Ab, or FITC-labeled mouse mAb TX21 (MBL International). At the end of the staining, silides were wased and incubated with 4′,6-diamidino-2 phenylindole (DAPI) for nuclear staining (molecular Probes).

To examine how PV is incorporated into the lymphoid organ, the sections were stained with an anti-poliovirus antibody (II-MAP-01, Japan Poliomyelitis Research Institute) for 15 min. The sections were then incubated with TRITC-labeled goat anti-mouse IgG (Jackson Immunoresearch Laboratories) for 15 min. Finally, the sections were stained with FITC-labeled mouse mAb TX21. After the staining, slides were washed and analyzed with a Keyence Biozero BZ-8000.

Scanning electron microscopy (SEM). The tissue samples were rinsed in phosphate-bu ered saline with 0.1 M sucrose (pH 7.4) and postfixed with 1% osmium tetroxide in 0.1 M phosphate bu er at 4 C for 2 h. All the samples were dehydrated with 50:50, 70:30, 80:20, 90:10, and 95:5 ethanol/water mixtures and 100% ethanol for 10 min each and rinsed three times with 100% ethanol for further dehydration. The samples were critical-point dried by flooding with liquid carbon dioxide at 5 C for 20 min and then raising the temperature to the critical-point (JCPD-5, JEOL). For SEM, samples were sputter-coated with gold (JFC-1100E, JEOL) and examined with a JEOL JSM-5200 scanning electron microscope at an accelerating voltage of 15 kV.

Transmission electron microscopy (TEM). The tissue samples were rinsed in phosphate-bu ered saline with 0.1 M sucrose (pH 7.4) and postfixed with 1% osmium tetroxide in 0.1 M phosphate bu er at 4 C for 2 h. All the samples were rinsed briefly with 50:50, 70:30, 80:20, 90:10, and 95:5 ethanol/water mixtures and 100% ethanol for 10 min each and three

Please cite this article in press as: Y. Takahashi et al., Nonhuman primate intestinal villous M-like cells: ..., Biochem. Biophys. Res. Commun. (2008), doi:10.1016/j.bbrc.2008.01.120

times with 100% ethanol for dehydration, and then embedded in epoxy resin (Quatol 812). One micrometer sections were cut using a glass knife and then stained with toluidine blue. Suitable areas for ultrastructural study were chosen after examining 1 μm sections under a light microscope. Sections of 60–90 nm were cut on a Leica EM UC6 ultramicrotome using a diamond knife and sections were mounted on a copper grid and stained with 1% uranyl acetate and Reynolds lead citrate. The grids were examined under a JEOL JEM 1200-EX electron microscope.

Energy dispersive X-ray spectroscopy (EDS). EDS analysis, which was consigned to JEOL Datum Ltd., was performed to quantify PV by measuring gold concentration within a specimen.

Results

Intraintestinal inoculation site of PV in rhesus macaques

To elucidate the details of PV gut infection in rhesus macaques, an attenuated PV Sabin strain was carefully inoculated into the lumen of the ileum at 15 cm from the ileocecal valve (Fig. 1A). After inoculation, the terminal ileum tissue was subjected to light microscopy, immunofluorescence microscopy, SEM, and TEM. As shown in Fig. 1B, the largest Peyer's patch is found in the lumen of the terminal ileum in rhesus macaques. Light microscopy revealed the typical structure of a mucosal lymphoid follicle, composed of GCs and a dome area bulging into the lumen (Fig. 1C). Furthermore, SEM revealed that hemispherical domes were distributed between intestinal villi (Fig. 1D).

Comparison of CD155 expression in PPs between cynomolgus and rhesus macaques

To clarify the basis for the di erence in susceptibility to oral PV infection between humans and rhesus macaques, Iwasaki et al. assessed the expression pattern of CD155 in PPs of these species. The results suggested that the suboptimal expression of CD155 in the rhesus macaque FAE and the lack of expression in GCs in PPs may explain why rhesus macaques are not susceptible to oral infection. Therefore, it is intriguing to speculate that in cynomolgus macaques, which are susceptible to oral PV infection, CD155 is most likely optimally expressed in FAE and GCs in PPs. To determine CD155 expression in cynomolgus macaques, we performed immunofluorescence staining of PPs using anti-CD155 Abs. The expression of CD155 in GCs in PPs was prominent in the case of staining with mAb D171 (Supplementary Fig. S1A) and mAb TX21 (Supplementary Fig. S1B) but that in FAE was not prominent. These results indicate that the mAbs used in this experiment can specifically stain CD155 on cells in cynomolgus GCs.

Furthermore, we assessed whether CD155 is not expressed in rhesus macaque PPs. Unexpectedly, in rhesus macaques, the expression level of CD155 on cells within FAE and GCs is not significantly di erent from that observed in cynomolgus macaques (Fig. 1E and F; see the less intensely stained GCs depicted by the DAPI nuclear staining in Fig. 1F). Furthermore, anti-CD155 mAb (TX21) can also stain cells in GCs in di erent sections of rhesus macaque PPs (Supplementary Fig. S1E).

Inoculated PV was e ciently incorporated into rhesus macaque villi

To examine how PV is incorporated into the lymphoid organ, attenuated PV was inoculated into the rhesus macaque ileum. One hour after the injection, the tissue was subjected to immunofluorescence analysis. As shown in Fig. 1H, the virus was detected inside the villi but was hardly detected in GCs that were strongly stained by anti-CD155 mAb (Fig. 1G). A merged image of panels 1G and 1H is shown in panel 1I. As shown in Fig. 1I, the colocalization of PV and CD155 was prominent in LP (Fig. 1I). When PPs from a di erent section were further observed, the virus was clearly detected in the LP of villi (Fig. 1J). On the other hand, weak fluorescence was detected in the subepithelial dome region in PPs (Fig. 1J) although fluorescence was hardly detected in GCs. These results indicate that PV e ciently enters into the villi rather than GCs within PPs in rhesus macaques. It is highly possible that a cofactor involved in PV accumulation in GCs is lacking in rhesus macaques.

SEM and TEM of FAE-M Cells

To examine why PV is not e ciently transported into cells in GCs underneath FAE, we investigated whether there are no typical M cells in rhesus macaque PPs because it has been suggested that PV is transported into PPs via human M cells [9]. Microscopy at a low magnification revealed hemispherical domes that were distributed between intestinal villi (Fig. 1K). Among cells in FAE, there were a few M cells showing a typical depressed surface with short and irregular microvilli (Fig. 1L). Rhesus macaque M-cell microvilli were shorter, thicker and fewer in number than the microvilli of adjacent absorptive enterocytes (Fig. 1M). Furthermore, the M-cell cytoplasm was invaginated by migrating lymphoid cells (Fig. 1M). These results demonstrated that there are typical M cells in rhesus macaque FAE, although we cannot exclude the possibility that rhesus macaque M cells in PPs cannot e - ciently take up PV in comparison to human M cells.

SEM and TEM of villous M-like cells

To examine why PV is e ciently transported into LP, we investigated whether there are M-like cells in rhesus macaque villi because it has been demonstrated that intestinal villous M cells serve as a gateway for the antigen sampling of gut in mice [15]. SEM of rhesus macaque villous M-like cells revealed the hallmark feature of M cells, which is a typical depressed surface with short and irregular microvilli (Fig. 1N and O). TEM also showed villous M-like cells (Fig. 1P). Furthermore, infiltrating lymphocytes

Please cite this article in press as: Y. Takahashi et al., Nonhuman primate intestinal villous M-like cells: ..., Biochem. Biophys. Res. Commun. (2008), doi:10.1016/j.bbrc.2008.01.120

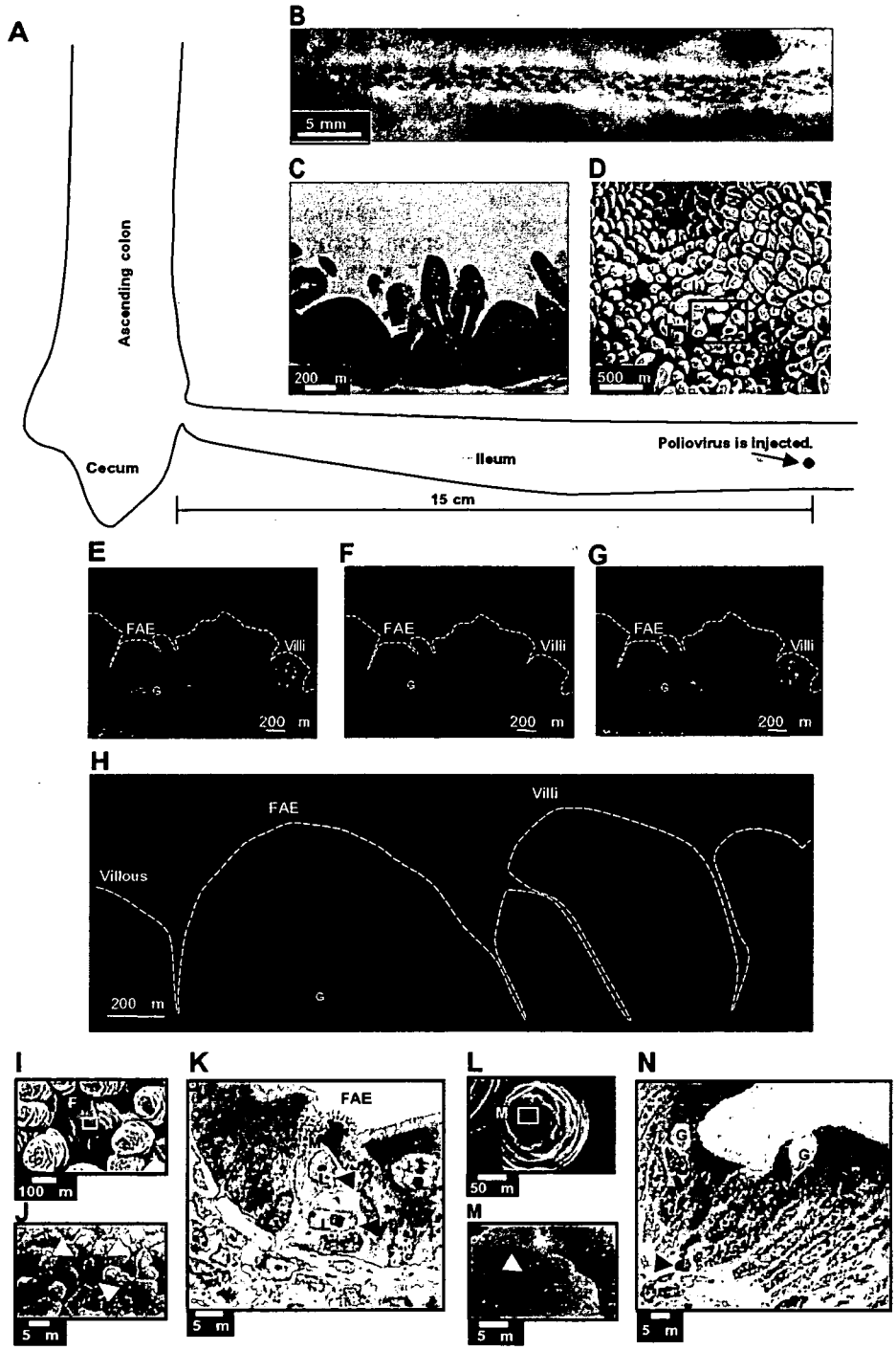

Fig. 1. PV is clearly detected in the lamina propria (LP) of villi. Attenuated PV was inoculated into the lumen of the ileum at 15 cm from the ileocecal valve (A). After inoculation, the parts of the ileum including the inoculation site and Peyer's patches (PPs) were collected (B). Hematoxylin–eosin staining of rhesus PPs (C). Scanning electron micrograph showing the ileum dome bulging into the gut lumen between intestinal villi (D). One hour after PV inoculation, the portion between the inoculation site of PV and the ileocecal valve was excised and subjected to immunofluorescence analysis. CD155 staining (E), PV staining (F), and merged (G) images are shown. (H) Di erent sections of rhesus macaque PPs were also stained by anti-PV mAb. PV can e ciently penetrate into the LP rather than into the subepithelial dome region. G, germinal center. SEM demonstrates that the M cells (I and J) in PPs and the villous M-like cells (L and M) in the villus epithelium are distinguishable from enterocytes by their relatively depressed and dark brush border (white arrowhead). TEM images of M cells in PP (K) and villous M-like cells in villi (N) show short stub like microvilli and the presence of infiltrating Q1 lymphocytes (L) in their pockets (black arrowhead). M, M cell or villous M-like cell.

Please cite this article in press as: Y. Takahashi et al., Nonhuman primate intestinal villous M-like cells: ..., Biochem. Biophys. Res. Commun. (2008), doi:10.1016/j.bbrc.2008.01.120

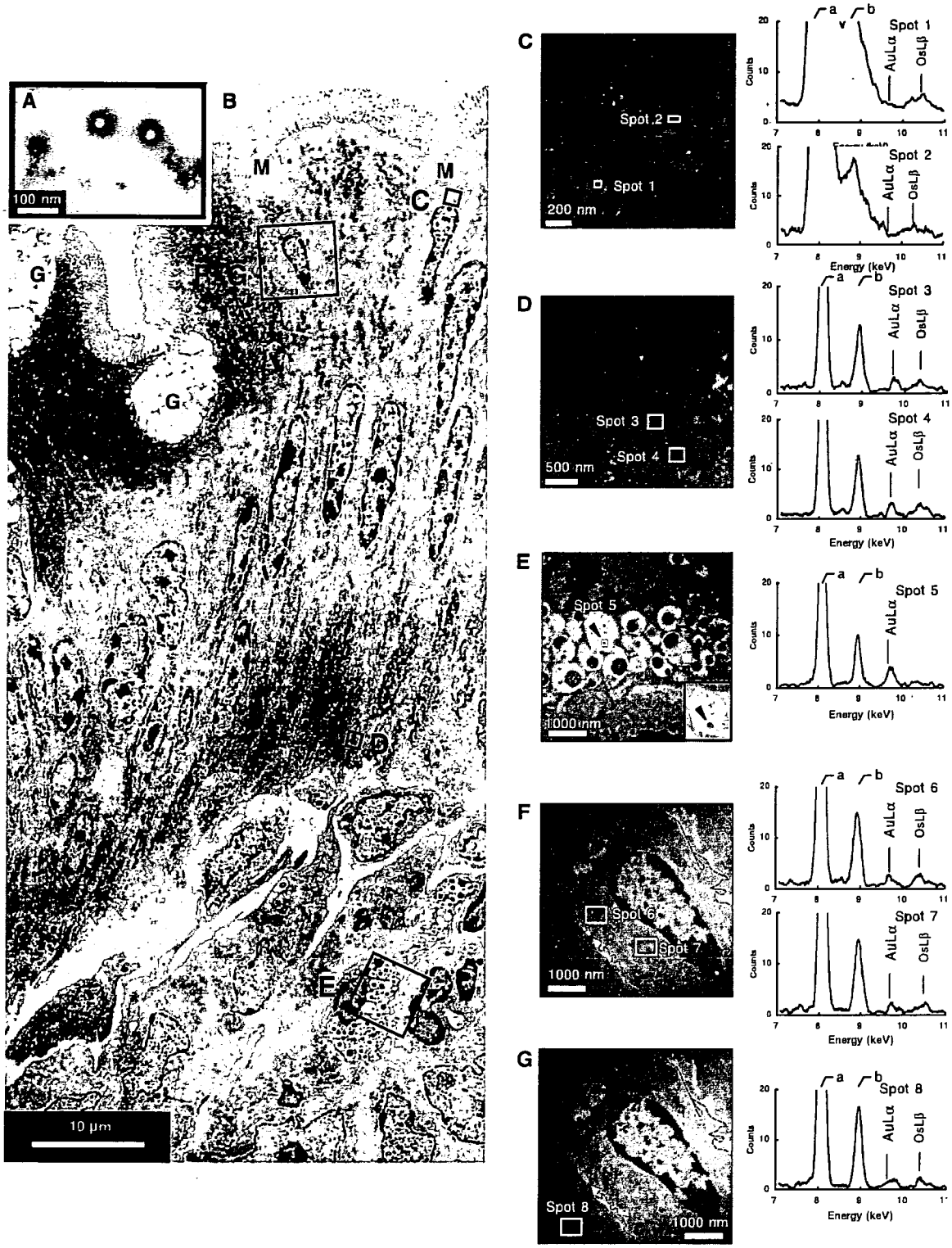

Fig. 2. PV can e ciently penetrate into villous M-like cells. PV was labeled with 5 nm gold particles and subjected to electron microscopies (A). A TEM view of villous epithelium (B) G, goblet cells; M, villous M-like cells. Panels (C–G) depict higher-magnification images of panel B for EDS. Graphs show EDS of spots (1–8) confirming the presence of gold particles (C–G). The a and b signals come from Cu (8.040 and 8.904 keV) that is attributed to the sample holder, and the b signal also contains the signal of OsLα (8.910 keV). The intensities of background signals from spots 1 and 2 in panel C were higher than those from other spots from panels D–G because spots 1 and 2 were on the TEM Cu-grid.

Please cite this article in press as: Y. Takahashi et al., Nonhuman primate intestinal villous M-like cells: ..., Biochem. Biophys. Res. Commun. (2008), doi:10.1016/j.bbrc.2008.01.120

were also observed in the pockets of villous M-like cells (Fig. 1P). These results suggest that villous M-like cells may form an alternative gateway for PV and provide evidence that nonhuman primate M-like cells develop and localize in the villous epithelium as well as in the FAE of PPs.

Internalization of PV by villous M-like cells

To investigate whether rhesus macaque villous M-like cells can take up PV, the rhesus macaque ileum was inoculated with gold-labeled PV (Fig. 2A) and subjected to EDS. The advantage of EDS is that gold-labeled PV can be directly detected when PV is completely embedded in an ultrathin section. The characteristic X-ray peak from gold (AuL-alpha: approximately 9.712 keV) is used to confirm the presence of Nanogold within a section. Forty-five minutes after inoculation, EDS demonstrated the presence of gold-labeled PV in the basolateral cytoplasm (spots 3 and 4; Fig. 2B and D) but not in the apical cytoplasm (spots 1 and 2; Fig. 2B and C) of villous M-like cells. In addition, gold-labeled PV was also specifically engulfed by macrophage-like cells in LP (spots 5; Fig. 2B and E). As shown in the insert of Fig. 2E, a PV particle was clearly and directly detected. Furthermore, we examined whether the adjacent M-like cells also take up PV (spots 6 and 7; Fig. 2B and F). Results revealed the localization of PV beside the nucleus (Fig. 2F). In contrast, there is no signal corresponding to PV in an adjacent epithelial cell (spot 8; Fig. 2G). Taken together, these results indicate that rhesus macaque villous M-like cells have the ability to take up PV from the lumen.

Discussion

The premise of oral PV infection in humans postulates that CD155 is expressed not only on enterocytes in FAE but also on cells in GCs [4]. If so, cynomolgus epithelial cells in FAE and cells in GCs should express CD155 because cynomolgus macaques are susceptible to infection by PV administered orally. We searched for CD155 in PPs in cynomolgus macaques. Staining with CD155-specific mAbs (D171 and TX21) revealed that CD155 was highly expressed not only on enterocytes in FAE but also on cells in GCs.

However, not much has been known about the PV infection patterns in the gut of rhesus macaques so far. We examined whether CD155 is indeed not expressed within rhesus macaque GCs and whether PV is indeed not incorporated into rhesus macaque intestinal lymphoid tissue. Unexpectedly, staining with CD155-specific mAbs (D171 and TX21) revealed that rhesus macaque CD155 was highly expressed not only on cells in GCs but also on those in LP. Furthermore, our immunofluorescence analysis indicated that PV is e ciently incorporated into LP in the villi rather than into GCs. These findings suggest that in rhesus macaques, an as yet unidentified factor is required for the translocation of PV into GCs after PV penetrates into FAE-M cells, and that there are cells that function similarly to FAE-M cells as a gateway for PV on villi.

A recent study [15] has directly demonstrated the function of mouse villous M cells as a gateway for bacteria. The morphological characteristics of the rhesus macaque FAE-M cells in ileal PPs were previously reported [16], but to our knowledge, our present study is the first to show the function of nonhuman primate villous M-like cells as a gateway for PV. Rhesus macaque villous M-like cells were distinguishable from intestinal villous epithelial cells on the basis of the criteria including (i) short and irregular microvilli, (ii) endocytic activity and ability to take up PV as well as macromolecules, and (iii) an intraepithelial pocket that allows a cluster of lymphocytes to be located in the FAE of PPs; currently, there is no reliable identified antigen marker that can be used to positively identify primate villous M cells. Indeed, EDS analysis demonstrated that PV was internalized within villous M-like cells and transported into LP.

Acknowledgment

Both attenuated PV (Sabin Strain) and anti-PV Ab were obtained from the Japan Poliomyelitis Research Institute.

Appendix A. Supplementary data

Supplementary data associated with this article can be found, in the online version, at doi:10.1016/j.bbrc.2008.01.120.

References

[1] A.B. Sabin, R. Word, The natural history of human poliomyelitis: I. Distribution of virus in nervous and non-nervous tissues, J. Exp. Med. 73 (1941) 771–793.
[2] D. Bodian, Emerging concept of poliomyelitis infection, Science 122 (1955) 105–108.
[3] G.D. Hsiung, B.D. Black, J.R. Henderson, Susceptibility of primates to viruses in relation to taxonomic classification, in: J. Buettner-Janusch (Ed.), Evolutionary and Genetic Biology of Primates, vol. II, Academic Press, New York, NY, 1964, pp. 1–23.
[4] A. Iwasaki, R. Welker, S. Mueller, M. Linehan, A. Nomoto, E. Wimmer, Immunofluorescence analysis of poliovirus receptor expression in Peyer's patches of humans, primates, and CD155 transgenic mice: implications for poliovirus infection, J. Infect. Dis. 186 (2002) 585–592.
[5] S. Koike, C. Taya, T. Kurata, S. Abe, I. Ise, H. Yonekawa, A. Nomoto, Transgenic mice susceptible to poliovirus, Proc. Natl. Acad. Sci. USA 88 (1991) 951–955.
[6] R.B. Ren, F. Costantini, E.J. Gorgacz, J.J. Lee, V.R. Racaniello, Transgenic mice expressing a human poliovirus receptor: a new model for poliomyelitis, Cell 63 (1990) 353–362.
[7] S. Zhang, V.R. Racaniello, Expression of the poliovirus receptor in intestinal epithelial cells is not su cient to permit poliovirus replication in the mouse gut, J. Virol. 71 (1997) 4915–4920.
[8] S. Ohka, H. Igarashi, N. Nagata, M. Sakai, S. Koike, T. Nochi, H. Kiyono, A. Nomoto, Establishment of a poliovirus oral infection system in human poliovirus receptor-expressing transgenic mice that are deficient in alpha/beta interferon receptor, J. Virol. 81 (2007) 7902–7912.

Please cite this article in press as: Y. Takahashi et al., Nonhuman primate intestinal villous M-like cells: ..., Biochem. Biophys. Res. Commun. (2008), doi:10.1016/j.bbrc.2008.01.120

[9] P. Sicinski, J. Rowinski, J.B. Warchol, Z. Jarzabek, W. Gut, B. Szczygiel, K. Bielecki, G. Koch, Poliovirus type 1 enters the human host through intestinal M cells, Gastroenterology 98 (1990) 56–58.
[10] A. Frey, K.T. Giannasca, R. Weltzin, P.J. Giannasca, H. Reggio, W.I. Lencer, M.R. Neutra, Role of the glycocalyx in regulating access of microparticles to apical plasma membranes of intestinal epithelial cells: implications for microbial attachment and oral vaccine targeting, J. Exp. Med. 184 (1996) 1045–1059.
[11] J.P. Kraehenbuhl, M.R. Neutra, Epithelial M cells: di erentiation and function, Annu. Rev. Cell Dev. Biol. 16 (2000) 301–332.
[12] M.R. Neutra, A. Frey, J.P. Kraehenbuhl, Epithelial M cells: gateways for mucosal infection and immunization, Cell 86 (1996) 345–348.
[13] M.R. Neutra, N.J. Mantis, A. Frey, P.J. Giannasca, The composition and function of M cell apical membranes: implications for microbial pathogenesis, Semin. Immunol. 11 (1999) 171–181.
[14] R.L. Owen, Sequential uptake of horseradish peroxidase by lymphoid follicle epithelium of Peyer's patches in the normal unobstructed mouse intestine: an ultrastructural study, Gastroenterology 72 (1977) 440–451.
[15] M.H. Jang, M.N. Kweon, K. Iwatani, M. Yamamoto, K. Terahara, C. Sasakawa, T. Suzuki, T. Nochi, Y. Yokota, P.D. Rennert, T. Hiroi, H. Tamagawa, H. Iijima, J. Kunisawa, Y. Yuki, H. Kiyono, Intestinal villous M cells: an antigen entry site in the mucosal epithelium, Proc. Natl. Acad. Sci. USA 101 (2004) 6110–6115.
[16] E.M. Kuhn, F.J. Kaup, Morphological characteristics of the ileal Peyer's patches in the rhesus macaque: a histological and ultrastructural study, Anat. Histol. Embryol. 25 (1996) 65–69.

Please cite this article in press as: Y. Takahashi et al., Nonhuman primate intestinal villous M-like cells: ..., Biochem. Biophys. Res. Commun. (2008), doi:10.1016/j.bbrc.2008.01.120

Human Immunodeficiency Virus-Induced Apoptosis of Human Breast Cancer Cells *Via* CXCR4 is Mediated by the Viral Envelope Protein But Does Not Require CD4

Masafumi Endo, Asako Inatsu, Koji Hashimoto, Nobutoki Takamune, Shozo Shoji and Shogo Misumi*

Department of Pharmaceutical Biochemistry, Faculty of Medical and Pharmaceutical Science, Kumamoto University, 5-1 Oe-Honmachi, Kumamoto 862-0973, Japan

Abstract: HIV-1 infection results in an increased risk of malignancy as well as immune suppression. However, analyses of cancer incidence in chronically immunosuppressed transplant recipients and HIV-infected person have demonstrated an unexpected low incidence of certain types of cancer, such as breast cancers, and the mechanism behind this remains unclarified. In this study, we show that most breast cancer cell lines express CXCR4 but are not susceptible to HIV-1 infection. The apoptosis of breast cancer cells is induced by HIV-1 in a viral-dose- and time-dependent manner without productive infection. The apoptosis is induced by R5X4 and X4 HIV-1 but not by R5 HIV-1, and is inhibited by an anti-CXCR4 antibody, an anti-gp120 antibody, AMD3100, or pertussis toxin. The apoptosis is mediated *via* CXCR4 in breast cancer cells that exhibit conformational heterogeneity in comparison with CXCR4 in T-cells. Furthermore, the gp120 mutant (E370R) with a low CD4 binding ability can specifically induce apoptosis in breast cancer cells but not in T-cells. Taken together, these results indicate that HIV-1 and gp120 can induce breast cancer cell apoptosis through gp120-CXCR4 interaction without a CD4-induced conformational change of gp120, and may lead to a novel HIV-1-based therapy for breast cancer.

Keywords: Breast cancer, HIV-1 envelope protein, apoptosis, CXCR4.

Human immunodeficiency virus type 1 (HIV-1) infection is associated with the depletion of $CD4^+$ T-cells. The phenomenon renders the host susceptible to opportunistic infections through the dysregulation and dysfunction of the immune system [1, 2]. HIV-1 infection also results in an increased susceptibility to malignant tumors caused by a decreased immunologic response to tumor cells and an increased susceptibility to oncogenic viral infection [3, 4]. Indeed, people infected with HIV are at a high risk of developing cancer [5-7]. Cancers in HIV-1-infected patients can be divided into three groups. The first group includes AIDS-defining cancers such as Kaposi's sarcoma [7]. The second group includes malignancies more prevalent among patients with HIV infection such as Hodgkin's lymphoma, squamous cell carcinoma of the anus, and lung cancer [5, 8-10]. The third group includes cancers whose incidences are not increased by HIV infection such as breast cancer [10-12]. Several hypotheses explaining the low incidence of breast cancer among HIV-1-infected patients have been proposed (e.g., immunodeficiency, socioeconomic state, racial disparity, metabolic complications of antiretroviral therapy, and a short life span of HIV-1-infected patient) [10-15].

HIV-1 uses CD4 and a chemokine receptor for cellular entry [16]. After the binding of the HIV-1 envelope glycoprotein (Env) gp120 to CD4, gp120 changes its conformation to bind to the chemokine receptor and initiates fusion with the cellular membrane. The chemokine receptors CCR5 and CXCR4 are the main coreceptors for the cellular entry of HIV-1. In general, viral strains are classified into R5, X4 and R5X4 according to the usage of chemokine receptor [17]. The HIV-1 R5 virus is generally transmitted and predominates at the early stage of HIV-1 infection. In contrast, R5X4 and X4 viruses emerge at the later stage of infection, and their emergence is frequently associated with a rapid depletion of $CD4^+$ T-cells [18, 19].

Besides the viral entry, the binding of virion-associated gp120 to coreceptors induces physiological effects that are relevant to pathogenesis. In particular, the binding of gp120 to CCR5 [20-22] or CXCR4 [22, 23] was shown to trigger the apoptosis of both infected and uninfected T-cells, which represents a fundamental mechanism of immunodeficiency syndrome. HIV-1 isolates differ in their ability to induce the apoptosis of bystander uninfected cells and infected cells themselves, and apoptosis determinants seem to be located in gp120 [24, 25]. Although the precise regions in gp120 that can induce apoptosis have not been identified yet, HIV-1 gp120, which interacts with CXCR4, seems to have highly cytopathic effects because CXCR4 is expressed in a wide range of target cells [26-28].

CXCR4 has recently been shown to be expressed on primary tumours of human invasive lobular or ductal breast carcinoma and to mediate organ-specific metastasis [29, 30]. Therefore, we investigated the biological effect of HIV-1 on breast cancer cells. In this study, we observed the HIV-1-induced apoptosis of breast cancer cells without productive infection. Furthermore, the induction of apoptosis was critically dependent on the interaction of gp120 with CXCR4 without a CD4-induced conformational change of gp120.

*Address correspondence to this author at the Department of Pharmaceutical Biochemistry, Faculty of Medical and Pharmaceutical Science, Kumamoto University, 5-1 Oe-Honmachi, Kumamoto 862-0973, Japan; Tel: +81-96-371-4362; Fax: +81-96-362-7800;
E-mail: misumi@gpo.kumamoto-u.ac.jp

1570-162X/08 $55.00+.00

The gp120 mutant E370R specifically induces the apoptosis of breast cancer cells but not T-cells. These results indicate the possibility of developing a novel HIV-1-based breast cancer therapy.

MATERIAL AND METHODS

Cell Culture and HIV-1 Preparations

Human T lymphoblastoid cell lines (CEM, CEM-CCR5 and Molt4#8), a chronically HIV-1-infected T-cell line (CEM/LAV-1), and human breast cancer cell lines (MCF-7, and DU4475) were maintained at 37°C in the RPMI-1640 medium supplemented with 10% fetal calf serum (FCS) containing 100 IU/ml penicillin and 100 μg/ml streptomycin in 5% CO_2. The human breast cancer cell lines (MDA-MB-453 and MDA-MB-231) were maintained at 37°C in Dulbecco's modified Eagle's medium (DMEM) supplemented with 10% FCS containing 100 IU/ml penicillin and 100 μg/ml streptomycin in 5% CO_2.

For the preparation of infectious HIV-1, supernatants of the culture media of acutely HIV-1-infected cells (CEM-CCR5 for the JRFL strain, and CEMx174 for the 89.6 strain) and chronically HIV-1-infected T-cells (CEM/LAV-1 for the LAV-1 strain) were separately filtered through 0.45-μm-pore-size filters. The viral preparation was stored at –80°C until use.

Flow Cytometry

To compare the expression level of CD4 or CXCR4, cells (1×10^5) were washed with washing buffer (PBS containing 2% FCS and 0.02% NaN_3) and incubated with 10 μg/ml primary antibody (Leu-3a (Becton Dickinson Immunocytometry System), 12G5 (R & D Systems), 44717.111 (R & D Systems), IA2F9 [31], or the anti-CXCR4 N-terminal rabbit polyclonal antibody (Affinity BioReagents, Inc.) for 30 min at 4°C. The cells were then washed with the same washing buffer and incubated with suitable FITC-labeled secondary antibodies. The cells were washed again, and analyzed using an EPICS XL flow cytometer (Beckman Coulter).

Determination of Chemokine Receptor by SYBR Green Real-Time PCR Analysis

To determine CXCR4 expression in the breast cancer cell lines, total RNA of each cell line was extracted by the acid guanidinium phenol chloroform method using an ISOGEN kit (Nippon Gene). The extracted total RNA was reverse-transcribed to cDNA using Moloney-Murine Leukemia Virus Reverse Transcriptase and the Oligo-dT primer (Parkin Elmer, Roche Molecular Systems, Inc.). SYBR green real-time PCR analysis was performed using a DNA Engine Opticon 2 fluorescence detection system (MJ Research) and a DyNAmo HS SYBR green qPCR kit (MJ Research) according to the manufacturer's instructions. The primer pair of *human CCR5* (5'-GGACCAAGCTATGCAGGTGAC-3' and 5'-TTGGCACTGTGCTTTTGGAA-3') was used. PCR amplification was carried out using the following cycles: one cycle of 15 min at 95°C and 40 cycles in four steps for each (95°C for 10s, 57°C for 20s, 72°C for 20s, and 76°C for 2s). At the end of the cycles, melting temperature analysis was performed by gradually increasing temperature (0.5°C/s) to 95°C.

Detection of p24 Antigen and Total Viral DNA

To investigate whether breast cancer cells are actually resistant to HIV-1 infection, CEM cells (1×10^5), DU4475 and MCF7 cells (1×10^5) were inoculated with HIV-$1_{LAV\text{-}1}$ or HIV-$1_{89.6}$ (100 ng of the HIV-1 p24 antigen) and incubated at 37°C for 2h. The cells were washed twice and cultured at 37°C for 10 days. Then the culture supernatant of each cell line was collected, and p24 antigen level was measured by antigen-capture enzyme-linked assay using a RETRO-TEK HIV-1 p24 antigen enzyme-linked immunosorbent assay kit (ZeptoMetrix Corp.) according to the manufacturer's instructions. For the detection of total viral DNA, total DNA obtained after the purification procedure was subjected to SYBR green real-time PCR analysis as described above. The following primer pair was used: HIV-1 *pol* (5'-TACAGGAGCAGATGATACAG-3' and 5'-CCTG GCTTTAATTTTACTGG-3').

Annexin-V Staining Assay

To detect the annexin V-positive cells, an Annexin V-FLUOS staining kit (Roche Diagnostics GmbH) was used according to the manufacturer's recommendation. DU4475 and MCF-7 cells (1×10^6) were plated in 24-well plates and preincubated with or without increasing concentrations of pertussis toxin (SIGMA). This was followed by treatment with HIV-1 (100 ng of the HIV-1 p24 antigen) and incubation in 1 ml of a fresh medium at 37°C for 36h. Then the cells were harvested and resuspended in 100 μl of staining solution (containing annexin V-fluorescein and propidium iodide), and were mixed gently and incubated for 15 min at room temperature (15-25°C) in the dark. The samples were analyzed in an EPICS XL flow cytometer (Beckman Coulter).

Coculture Assay

Cocultivation of MCF-7 cells was carried out in a transwell to show whether gp120 induced apoptosis *via* CXCR4. HEK293 cells were transfected with a vector-derived mRNA (control), or an mRNA encoding HIV-$1_{89.6}$ gp120 WT or gp120 mutant (E370R). In the lower chamber, MCF-7 (1×10^6) or CEM (1×10^6) cells were incubated with HEK293 cells, which were placed in the upper chamber of a 3-μm-pore-size transwell (Corning, NY). After 48h of coculture, MCF-7 or CEM cells were subjected to Annexin-V staining assay.

TUNEL Assay

To detect the TUNEL-positive cells, DU4475 and MCF-7 cells (1×10^6) were washed with phosphate-buffered saline (PBS), and then preincubated with or without 20 μl of an anti-CD4 antibody (Leu-3a; Becton Dickinson Immunocytometry System), 5 μg of an anti-CXCR4 antibody (12G5; R & D Systems), or 2 μM AMD3100 (NIH AIDS Research and Reference Reagent Program) on ice for 30 min. The cells were then inoculated with HIV-1 (100 ng) preincubated with or without 5 μg of a cross-reactive anti-gp120 antibody (ImmunoDiagnostics), and cultured in 5 ml of a fresh medium at 37°C for 36h. Then the cells were harvested and subjected to an assay using a DeadEnd Fluorometric TUNEL system (Promega Corporation) according to the manifacturer's instructions.

RESULTS

Profiles of CXCR4 and CD4 Expressions on Breast Cancer Cells

The expression of either CCR5 or CXCR4 is one of the indicators of the susceptibility of $CD4^+$ target cells to HIV-1 infection [16]. Flow cytometry showed that CXCR4 was expressed on breast cancer cell lines (Fig. **1A**) and CD4 was expressed at a high level on Molt4#8 cells, but not on DU4475 and MCF-7 cells (Fig. **1B**). Furthermore, the RNA expression levels of CCR5 determined by quantitative real-time PCR analysis showed that most of the breast cancer cell lines have low or undetectable levels of CCR5 expression (data not shown).

Breast Cancer Cells are Resistant to HIV-1 Infection

Because CD4 is the primary receptor for the cellular entry of HIV-1, the absence of CD4 expression on breast cancer cells implies that they are resistant to HIV-1 infection. To investigate whether breast cancer cells are actually resistant to HIV-1 infection, conventional infection assays measuring HIV-1 proviral DNA and the HIV-1 p24 antigen were performed. DU4475 and MCF-7 cells were inoculated with HIV-1_{LAV-1}, which utilizes CXCR4 and CD4 for cellular entry, and incubated for 10 days. In human T lymphoblastoid CEM cells, HIV-1 total DNA was detected (Fig. **1C**) and abundant progeny virus was produced (Fig. **1D**). On the other hand, the total viral DNA level in breast cancer cells was less than 1/1000 that in CEM cells (Fig. **1C**) and the p24

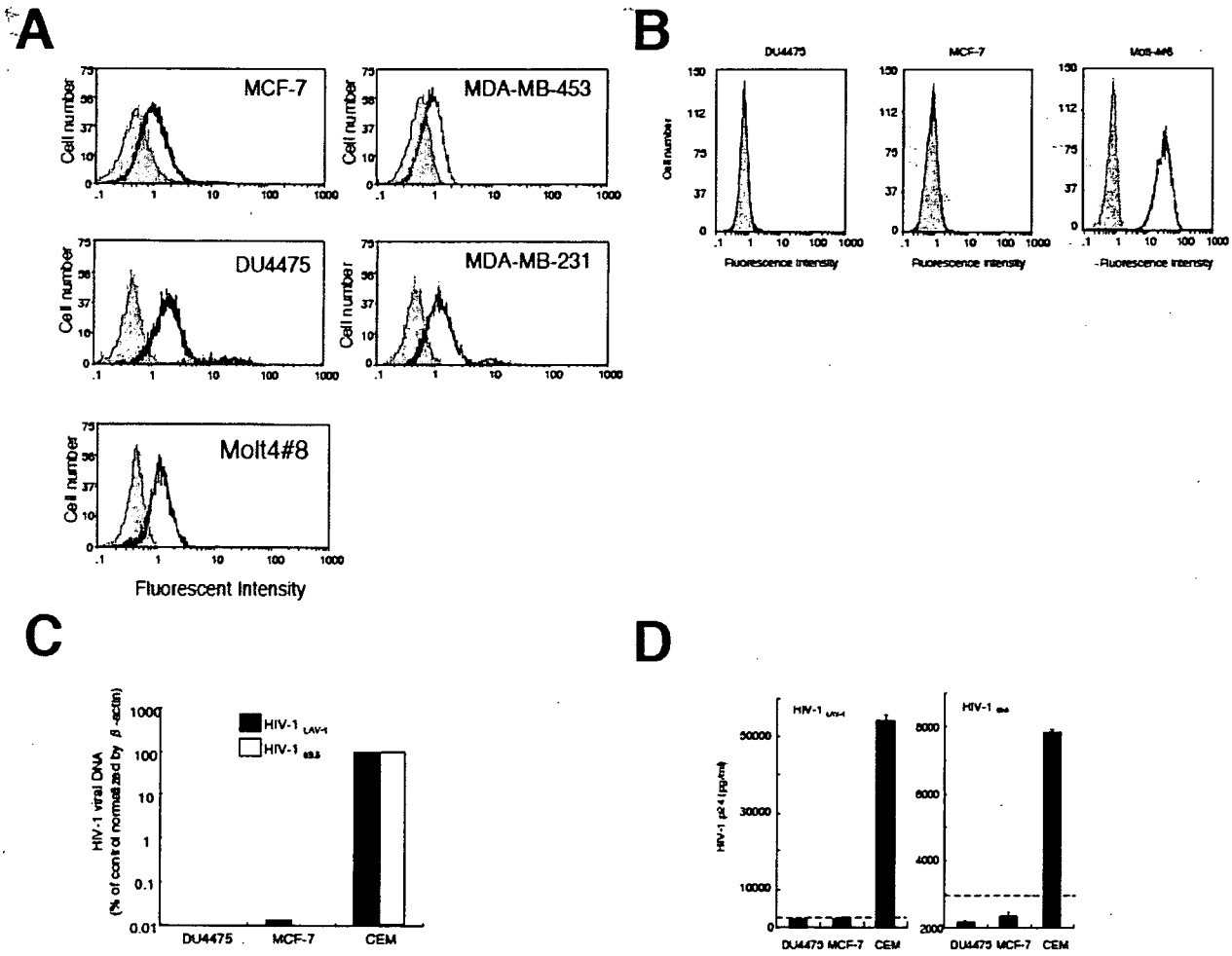

Fig. (1). Breast cancer cells are resistant to HIV-1 infection. (**A**) Human T-cell line (Molt4#8) and breast cancer cell lines (MCF-7, DU4475, MDA-MB-231 and MDA-MB-453) were incubated with 10 μg/ml anti-CXCR4 *N*-terminal (bold line) or isotype control (gray area). Subsequently, cells were incubated with suitable FITC-labeled secondary antibodies, and subjected to flow cytometry. (**B**) DU4475 and MCF-7 cells, and Molt4#8 cells were incubated with the anti-CD4 antibody (bold line) or the isotype control (gray area) for 30 min at 4°C. Subsequently, the cells were incubated with FITC-conjugated anti-mouse IgG and subjected to flow cytometry. CD4 is expressed at a high level on Molt4#8 cells, but not on DU4475 and MCF-7 cells. (**C**,**D**) DU4475 and MCF-7 cells, and CEM cells were inoculated with HIV-1_{LAV-1} or HIV-$1_{89.6}$ (100 ng of the HIV-1 p24 antigen). HIV-1 total DNA (**C**) and the p24 antigen level of supernatant (**D**) were measured by quantitative real-time PCR analysis and antigen-capture enzyme-linked assay as described in Materials and Methods. Dotted line in Fig. (**1D**). indicates the limit of p24 detection in this assay.

antigen level in the culture medium was below the detection limit (Fig. **1D**). Similar results were observed in experiments using HIV-$1_{89.6}$ (Fig. **1C,D**), suggesting that breast cancer cells are resistant to HIV-1 infection. These results were also consistent with an *in vivo* study [32] that demonstrated that breast cancer cells from HIV-1-infected patients are HIV-1-negative.

HIV-1 Induces Apoptosis of Breast Cancer Cells

In HIV-1-infected patients, many cell types are damaged by bystander apoptosis through several mechanisms and are involved in pathologic processes in these patients [22, 26, 33, 34]. To investigate the HIV-1-induced apoptosis of breast cancer cells, DU4475 cells were inoculated with HIV-$1_{89.6}$ at concentrations ranging from 62.5 to 500 ng of HIV-1 p24, incubated for 36h, and subjected to TUNEL assay to determine the percentage of apoptotic cells. The inoculation of DU4475 cells with increasing doses of HIV-1 showed that HIV-$1_{89.6}$ induced the apoptosis of DU4475 cells in a viral-dose-dependent manner (Fig. **2A**). Furthermore, the kinetics of HIV-1-induced apoptosis of DU4475 cells was also investigated. After the inoculation of cells with the virus (250 ng), the cells were subjected to TUNEL assay at different time points (0 to 36h). At incubation times longer than 12h, a significant apoptosis was observed and the percentage of apoptotic cells showed an almost linear relationship with time, suggesting that the HIV-1-induced apoptosis of breast cancer cells occurs in a time-dependent manner (Fig. **2B**). At 36h postinoculation, the percentage of apoptotic cells increased more than sevenfold. Taken together, these results indicate that HIV-1 affects the proliferation of breast cancer cells through the induction of their apoptosis.

Induction of Apoptosis of Breast Cancer Cells by HIV-1 is Dependent on Viral Isolate

The cytopathic effect of HIV-1 on bystander cells was diverse among viral strains and was dependent on several factors including viral coreceptor usage, the affinity between Env and the receptor, and the expression levels of CD4 and chemokine receptors on target cells [22, 24, 28]. To investigate the ability of diverse HIV-1 strains to induce the apoptosis of breast cancer cells, laboratory-adapted (X4 virus, HIV-1_{LAV-1}; R5 virus, HIV-1_{JRFL}; and R5X4 virus, HIV-$1_{89.6}$) or primary HIV-1 isolates (R5 subtype C virus, HIV-1_{MJ4}; X4 subtype A virus, HIV-$1_{92UG029}$; and X4 subtype C virus, HIV-$1_{98IN017}$) were inoculated to DU4475 and MCF-7 cells (Fig. **3**). The amount of inoculated virus was normalized to 100 ng of the p24 antigen, and the uninfected-cell supernatant was used as the control. TUNEL assay showed that HIV-1_{LAV-1} (X4) and HIV-$1_{89.6}$ (R5X4) significantly induced the apoptosis of DU4475 and MCF-7 cells (Fig. **3A,B**). However, HIV-1_{JRFL} (R5) did not exert any cytopathic effects on both cells (Fig. **3A,B**). In agreement with the finding, Annexin-V staining assay showed that the primary isolates HIV-$1_{92UG029}$ (X4A) and HIV-$1_{98IN017}$ (X4C) significantly induced the apoptosis of DU4475 and MCF-7 cells (Fig. **3C,D**). However, HIV-1_{MJ4} (R5C) did not exert any cytopathic effects on both cell lines (Fig. **3C,D**). These results indicate that the ability of HIV-1 to induce the apoptosis of breast cancer cells was dependent on the viral strain, and it seems that the laboratory-adapted (HIV-1_{LAV-1} and HIV-$1_{89.6}$) or primary X4 HIV-1 isolates (HIV-$1_{92UG029}$ and HIV-$1_{98IN017}$) are more potent inducers of apoptosis than the R5 HIV-1 isolates (HIV-1_{JRFL} and HIV-1_{MJ4}).

HIV-1 Induces Breast Cancer Cell Apoptosis Through gp120-CXCR4 Interaction

Because CXCR4 was expressed in DU4475 and MCF-7 cells (Fig. **1**), and R5X4 and X4 HIV-1 isolates were more potent inducers of the apoptosis of both cell lines (Fig. **3**), we hypothesized that the interaction of viral gp120 with CXCR4 might play critical roles in the induction of the apoptosis of breast cancer cells. To test this hypothesis, DU4475 and MCF-7 cells were preincubated with an anti-

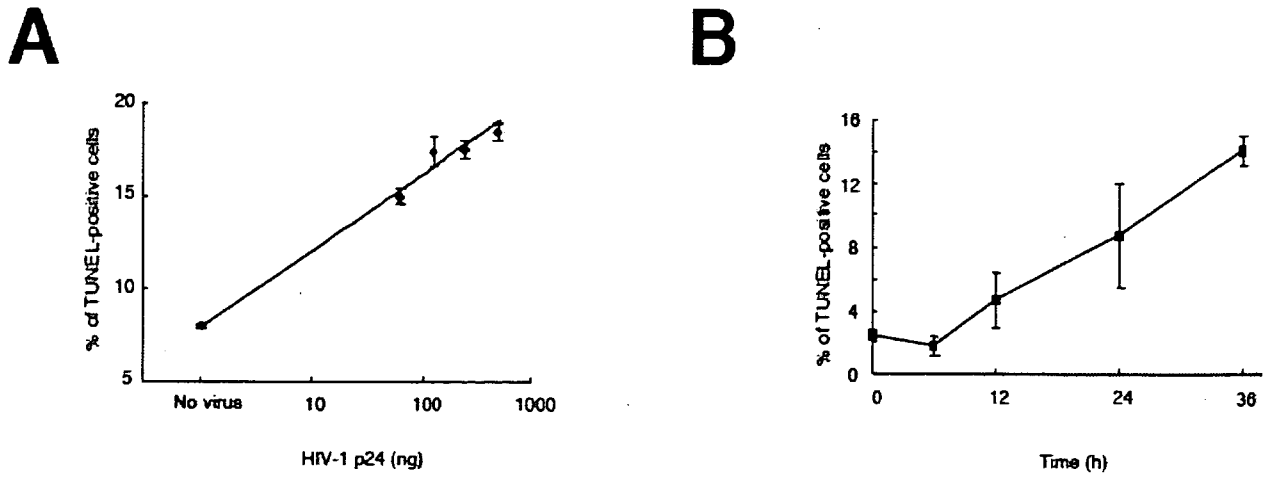

Fig. (2). HIV-1 induces apoptosis of breast cancer cells. To investigate the viral dose kinetics of apoptosis of breast cancer cells, DU4475 cells were inoculated with the culture supernatant of uninfected cells or various amounts of HIV-$1_{89.6}$ (62.5, 125, 250, 500 ng of the HIV-1 p24 antigen). After a 36h incubation, the cells were subjected to TUNEL assay to determine the percentage of apoptotic cells (**A**). To further investigate the time kinetics of apoptosis of breast cancer cells, DU4475 cells were inoculated with HIV-$1_{89.6}$ (250 ng of HIV-1 p24 antigen) and incubated for 0, 6, 12, 24 and 36h, and subsequently harvested and subjected to TUNEL assay to determine the percentage of apoptotic cells (**B**).

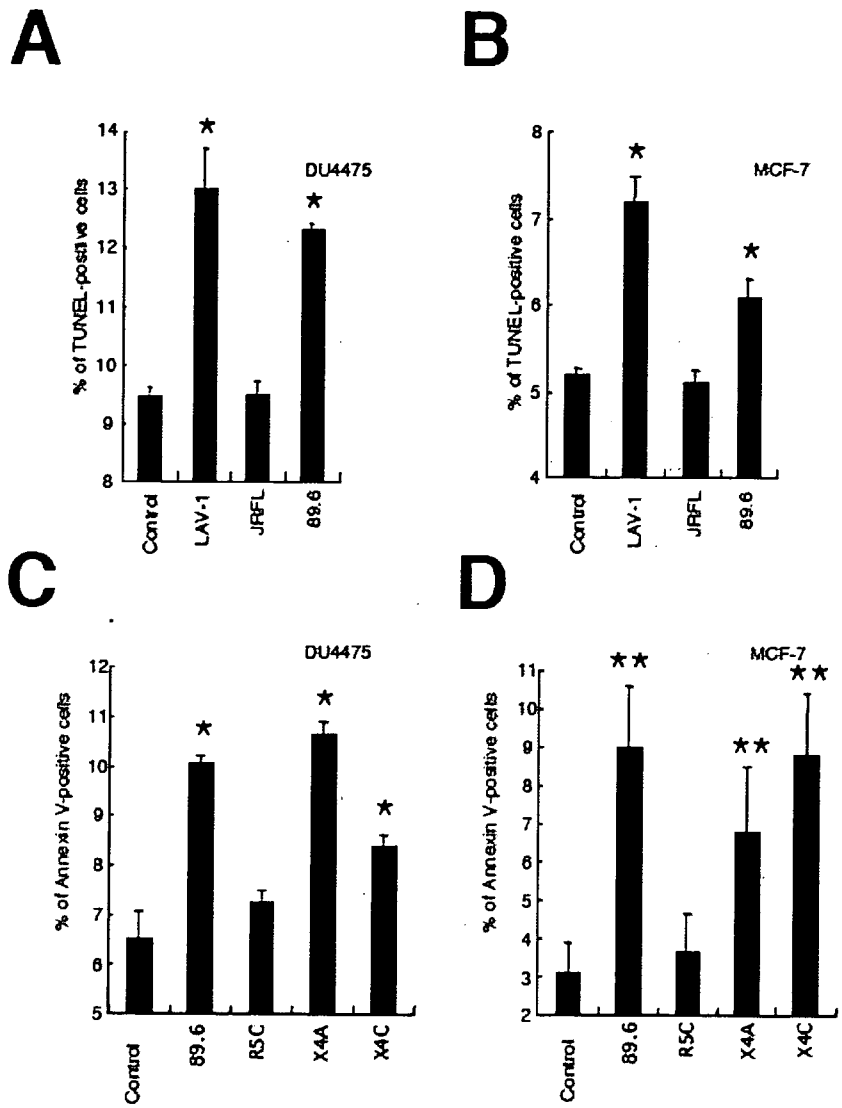

Fig. (3). Induction of apoptosis of breast cancer cells by HIV-1 is dependent on the HIV-1 phenotypic variants that are defined by their usage of CXCR4. DU4475 (**A**,**C**) and MCF-7 (**B**,**D**) cells were inoculated with the laboratory-adapted (X4 virus, HIV-1_{LAV-1}; R5 virus, HIV-1_{JRFL}; and R5X4 viruses, HIV-$1_{89.6}$) or primary HIV-1 isolates (R5 subtype C virus (R5C), HIV-1_{MJ4}; X4 subtype A virus (X4A), HIV-$1_{92UG029}$; and X4 subtype C viruses (X4C), HIV-$1_{98IN017}$). For the control, the culture supernatant of uninfected cells was used. After a 36h incubation, the cells were subjected to TUNEL (**A**,**B**) or Annexin-V staining assay (**C**,**D**) to determine the percentage of apoptotic cells (*$p<0.01$ compared with the control group, **$p<0.05$ compared with the control group (Dunnett's test following ANOVA)).

CD4 antibody, an anti-CXCR4 antibody, or a CXCR4 antagonist, AMD3100, while HIV-$1_{89.6}$ was also preincubated with a cross-reactive anti-gp120 antibody. The pretreatment of cells with 5 μg of the anti-CXCR4 antibody 12G5 and 2 μM AMD3100 significantly inhibited the apoptosis of DU4475 and MCF-7 cells (Fig. **4A**,**B**). In contrast, the pretreatment with the isotype control or the anti-CD4 antibody had no effect on the apoptosis of breast cancer cells (Fig. **4A**,**B**). Furthermore, the pretreatment of HIV-$1_{89.6}$ with 5 μg of the anti-gp120 antibody inhibited the apoptosis of breast cancer cells (Fig. **4A**,**B**) and HIV-$1_{89.6}$ gp120 induced the apoptosis of breast cancer cells (Fig. **4C**). Taken together, these results demonstrated that the interaction of HIV-1 gp120 with CXCR4 is required for the induction of the apoptosis of breast cancer cells.

Next, we studied which intracellular signals were involved in HIV-1-associated breast cancer apoptosis. Vlahakis *et al.* demonstrated that HIV gp120/CXCR4-mediated CD4 T lymphocyte death occurs independent of $G_{i\alpha}$ protein action [34]. To determine whether CXCR4 signaling in breast cancer cells is similar to that in T-cell apoptosis, MCF-7 cells were preincubated with the $G_{i\alpha}$ protein inhibitor pertussis toxin before incoculation with HIV-$1_{89.6}$. Interestingly, breast cancer cell death was effectively blocked by pertussis toxin, suggesting that HIV-1 gp120/CXCR4-